MODEL SYSTEMS FOR HETEROGENEOUS CATALYSIS: QUO VADIS SURFACE SCIENCE?

H.-J. Freund, N. Ernst, M. Bäumer, G. Rupprechter, J. Libuda,
H. Kuhlenbeck, T. Risse, W. Drachsel, K. Al-Shamery, H. Hamann
Fritz-Haber-Institut der Max-Planck-Gesellschaft
Department of Chemical Physics
Faradayweg 4-6, D-14195 Berlin

INTRODUCTION

Eighty to ninety percent of heterogeneous catalysts in use are either oxides or metals dispersed onto oxide supports [1]. Therefore, models must reflect this constitution. Our group has been active in preparing model systems for heterogeneous catalysts, including clean oxide surfaces [2] as well as deposited metal aggregate systems [3, 4]. We are using thin oxide films on metal substrates as samples to be able to apply the full scope of surface science methods to the study of model systems. Methods include those which are based on the analysis of charge carriers, as for example photoelectron spectroscopy, electron energy loss spectroscopy or scanning tunneling microscopy. However, also in connection with optical spectroscopy thin film systems are advantageous due to the high reflectance of the supporting metal. We restrict ourselves here to the discussion of results from our own laboratory and refer for a more complete overview of this field to review articles, which appeared in the literature recently [3-9]. We will cover a variety of different subjects including structural and morphological determinations in model catalyst systems as well as investigations of electronic properties, adsorption of molecules and reactivity studies.

While most of these results have been obtained under ultrahigh vacuum (UHV) conditions, we have recently made an attempt to extend these studies to higher pressures [10]. Thus, we are trying to close both the so called „materials gap“ by preparing model systems capturing essential features of real catalysts and the „pressure gap“ by moving from UHV to ambient conditions. Nevertheless, our basis are well defined UHV studies, and most of our conclusions heavily depend on a clear understanding of processes at clean surfaces.

One important aspect in using thin oxide film systems is the formation of the oxide overlayer on the metal substrate. Oxide formation and growth is a subject by itself, and not the central theme of this chapter. However, Wyn Roberts, to whom this chapter is dedicated, and his group have been interested in the initial stages of oxidation and oxygen induced chemistry on metal surfaces [11, 12], long before we became involved [13, 14]. Two quotations from one of his papers [15] document this: ”Interest in metal oxidation has led us to explore in 1963 how studies of the energy distributions of photoelectrons might provide definitive information on the transition of chemisorbed oxygen to an oxide overlayer with a discrete band structure.”, and then he goes on in the conclusions of the same paper: ”The significance of oxygen transients in providing low energy pathways in surface oxygenation reactions was first established using surface sensitive spectroscopies in conjunction with the probe-molecule approach.“

Roberts and his group have investigated a series of oxide overlayers with photoelectron spectroscopy, a technique that has been pioneered in its applications to surface studies in Cardiff [16-18]. NiO [19-21] is a prominent example for studies on oxides from the Roberts group. We will come back to other activities of this group concerning the chemistry of carbon dioxide in the course of the paper.

The present paper is organized as follows: We first present some results on clean oxide surfaces, and then proceed to deposited metal aggregates, discussing various specific aspects of nucleation and growth, diffusion, magnetic and electronic properties, adsorption and reactivity.

OXIDE SURFACES

The preparation of a clean oxide surface in ultrahigh vacuum is a rather difficult task. Strictly speaking, a certain oxygen activity is necessary in the gas phase to establish true equilibrium and then the stoichiometry is defined according to the chosen conditions [22]. In this respect, the oxide stoichiometry is not well-defined under dynamical UHV conditions, and the system is only kinetically stabilized. It is therefore believed that defects determine the physical and chemical properties of oxide surfaces. Particularly interesting are vanadium oxides and vanadylpyrophosphate compounds [23, 24]. Activation of hydrocarbons is thought to take place through abstraction of hydrogen atoms and the formation of surface hydroxyl groups involving defects and isolated transition metal oxide cluster sites [25].

We have started to study various vanadium oxide surfaces, V_2O_5, VO_2 [26] and V_2O_3 [27]. Figure 1 shows a photoemission spectrum of $V_2O_5(001)$ at the top which may be interpreted on the basis of calculations by Klaus Hermann and his group [28]. Briefly, the spectrum is dominated by O2p/O2s emissions and there is a minor admixture of the V3d wave

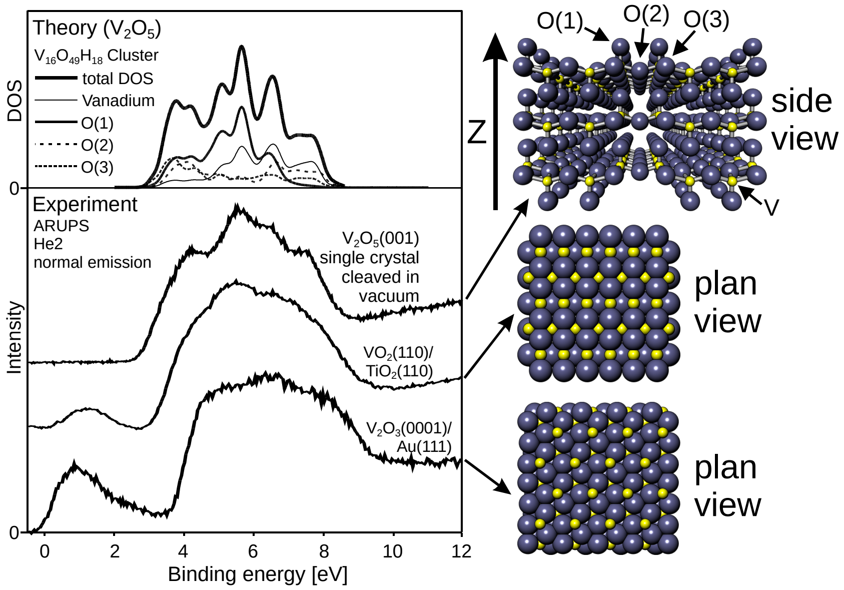

Figure 1. Photoelectron spectra and schematic representations of structures of various vanadium oxides [26, 27]. For comparison a computed density of states [28] is shown.

functions as indicated in the panel showing the results of the calculations. There are no features near the Fermi energy which would, if they were present, be characteristic for defects leaving V atoms in lower oxidation states. The oxygen derived part of the valence band can be separated into contributions from the various types of oxygens constituting the structure as shown in the right part of Fig. 1. The terminal vanadyl oxygen [O(1)] gives rise to the central features whereas the bridging oxygens [O(2) and O(3)] connecting the vanadyl groups are contributing to the wings of the valence band. We will use this fact to identify oxygen specific reactivity. The spectrum in the panel below V_2O_5 is that of VO_2. VO_2(110) has been grown as a thin film on the isostructural rutile(110) surface. The oxygen derived valence band is slightly different from that of V_2O_5. A characteristic difference is the appearance of a feature close to the Fermi edge in VO_2 indicating the presence of vanadium 3d electrons. Its intensity represents to some extent the population of the V3d orbitals. When we turn from VO_2 to V_2O_3 an even stronger increase in the V3d intensity is observed. In Fig. 1, in the lower panel, the valence band photoemission spectrum of V_2O_3(0001)/Au(111) is shown. The V_2O_3 film shows a sharp hexagonal LEED pattern representing the corundum type structure similar to Al_2O_3, Cr_2O_3 and Fe_2O_3 (see below). Again, the V_2O_3 oxygen valence band emission is not very characteristic, as compared with VO_2 and V_2O_5. It is only the change in the near Fermi edge structures that show a characteristic variation from V^{5+} to V^{3+}.

Vanadium pentoxide is rather inactive with respect to adsorbates. For example, molecular hydrogen only leads to observable effects in the

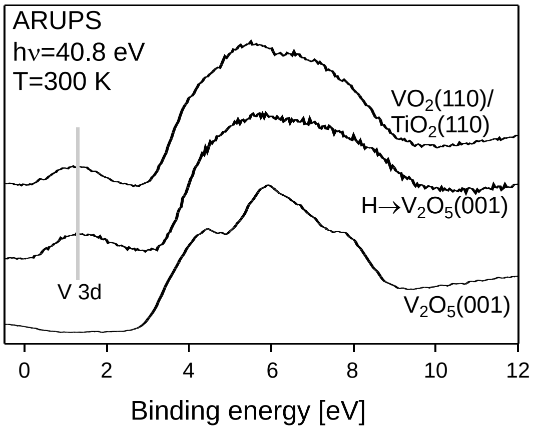

Figure 2. Photoelectron spectra of $V_2O_5(001)$ and $VO_2(110)/TiO_2(110)$ in comparison with a photoelectron spectrum obtained after dosing atomic hydrogen to a $V_2O_5(001)$ surface.

photoelectron spectrum after 10^4 L exposure. On the other hand, atomic hydrogen leads already at low exposure to recognizable changes in the photoelectron spectrum. The spectrum shown in Fig. 2 in the middle has been obtained after exposing the surface to atomic hydrogen. Opposite to the finding with molecular hydrogen the surface is chemically corroded. Defects form, as we also know from electron energy loss spectroscopy, and concomitantly reduced metal centers show up near the Fermi edge. In fact, the spectrum looks very similar to the one of VO_2 which we show for comparison. We have investigated the surface with vibrational spectroscopy and found no indication for the formation of hydroxyls. It is very likely, that during exposure water evolves from the surface. Still the complete absence of OH on the surface is surprising and might point to the formation of hydrogen vanadium oxide bronzes which are well-known to exist and which also have been used as precursors in the preparation of catalysts [29]. We are now starting to investigate reactivity of these surfaces to more complex molecules.

The best studied oxide surfaces are those of TiO_2, the rocksalt structures MgO and NiO as well as the corundum structured Al_2O_3, Cr_2O_3 and Fe_2O_3. Figure 3 shows the results of structural determinations for the three related systems $Al_2O_3(0001)$ [30], $Cr_2O_3(0001)$ [31, 32] and $Fe_2O_3(0001)$ [33]. In all cases a stable structure in UHV is the metal ion terminated surface retaining only half of the number of metal ions in the surface as compared to a full buckled layer of metal ions within the bulk [34]. The interlayer distances are very strongly relaxed down to several layers below the surface [2]. The perturbation of the structure of oxides due to the presence of the surface is considerably more pronounced than in metals, where the interlayer relaxations are typically of the order of a few percent. The absence of the screening charge in a dielectric material such as an oxide contributes to this effect considerably. It has recently been pointed out that oxide structures

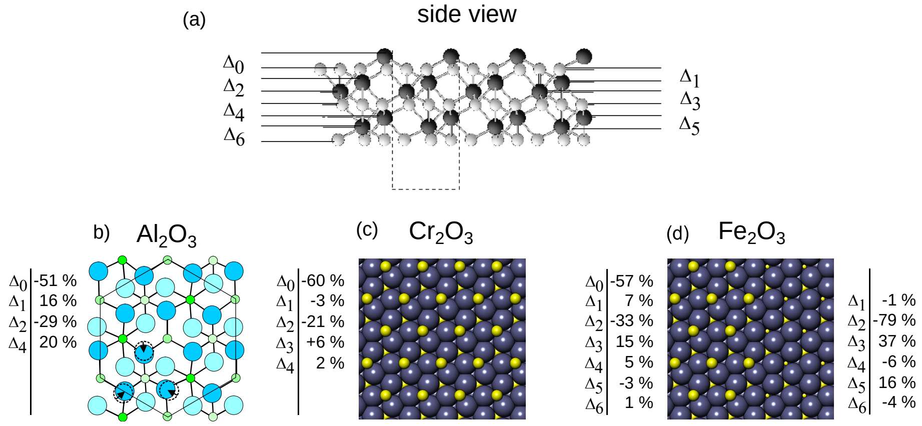

Figure 3. Experimental data on the structure of corundum-type depolarized (0001) surfaces (side and top views). Adapted from b) ref. [30], c) ref. [31, 32], d) ref. [33].

may not be as rigid as one might think judged on the relatively stiff phonon spectrum in the bulk [35, 36]. In fact, at the surface the phonon spectrum may become soft so that the geometric structure becomes rather flexible, and thus also very much dependent on the presence of adsorbed species [36].

The vibrational modes of a clean $Cr_2O_3(0001)$ surface have been studied under ultra high vacuum conditions with high resolution electron energy loss spectroscopy [36]. Figure 4 shows the spectrum of the clean surface at the bottom. A mode at 21.4 meV, which is confined to the first few atomic layers of the oxide, was detected, in addition to the Fuchs-Kliewer phonons. This mode shows only a very small isotopic shift when the $Cr_2O_3(0001)$ film is prepared from $^{18}O_2$ instead of $^{16}O_2$. In contrast to the Fuchs-Kliewer phonons which extend deeply into the bulk the 21.4 meV mode is very sensitive towards the presence of adsorbates, as is shown in Fig. 4. This can be seen by its attenuation upon exposure of the surface to CO, which in this case is only weakly adsorbed. Full-potential linearized augmented plane wave calculations [36] show that this mode is an in-phase oscillation of the second-layer oxygen atoms and the Cr atoms of the two layers below. A schematic representation of the mode is shown in the inset of Fig. 4.

Bulk oxide stoichiometries depend strongly on oxygen pressure, a fact that has been recognized for a long time and we have alluded to above [2]. So do oxide surfaces, structures and stoichiometries, a fact that has been shown again in a recent study on the $Fe_2O_3(0001)$ surface by the Scheffler and Schlögl groups [34]. In fact, if a Fe_2O_3 single crystalline film is grown in low oxygen pressure, the surface is metal terminated while growth under higher oxygen pressures leads to oxygen termination. This surface would be formally unstable on the basis of electrostatic arguments [2]. However, calculations by the Scheffler group have shown that a strong rearrangement of the electron distribution as well as relaxation between the layers leads to a stabilization of the system. STM images by Weiss and co-workers

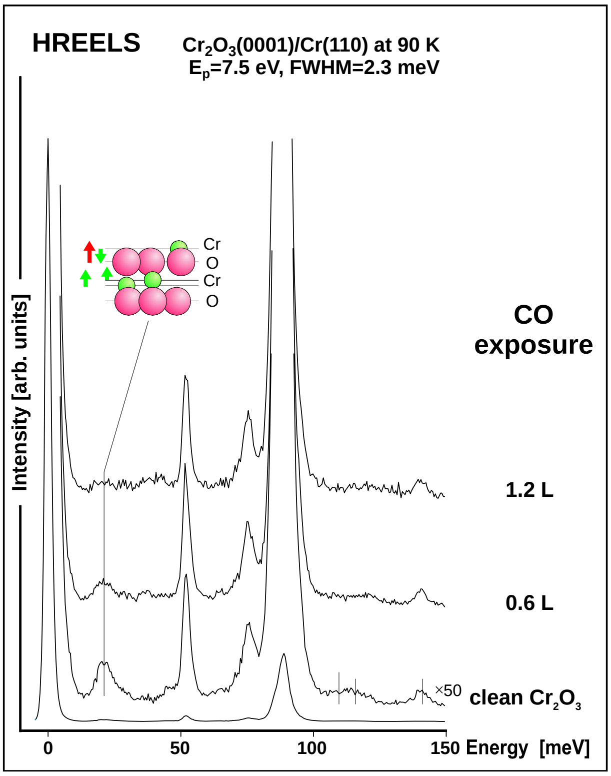

Figure 4. Electron energy loss spectra in the vibrational regime of clean and CO-covered Cr_2O_3(0001)/Cr(110) surface. [E_p: 7.5 eV, specular scattering] The inset shows a schematic representation of the calculated normal mode of a Cr_2O_3(0001) surface at 21.4 meV, according to ref. [36].

corroborate the coexistence of oxygen and iron terminated layers and thus indicate that stabilization must occur. Of course, there is need for further structural characterization. For the surface of Cr_2O_3(0001) infrared spectroscopic data suggest a different termination when the clean surface is exposed to oxygen [37]. Figure 5 shows the appearance of a sharp line which develops out of a broad feature after heating the surface to room temperature. As has been discussed earlier and also supported by isotopic labeling experiments by Dillmann et al. [37] chromyl groups are formed on the surface and it was suggested that the chromium ions in the surface layer of the clean surface bind oxygen to form such chromium-oxygen double bonds. As is obvious from Fig. 5, there are adsorbed oxygen precursors to the chromyl formation. The width as well as frequency is indicative of an O_2^- species being adsorbed on the surface in a more or less upright position [37]. The chemistry of this species has yet to be investigated.

CO adsorption on corundum type (0001) surfaces is interesting because, opposite to checker board rocksalt type surfaces, on the (0001) surface of Cr_2O_3 CO has been shown to assume a strongly inclined almost flat

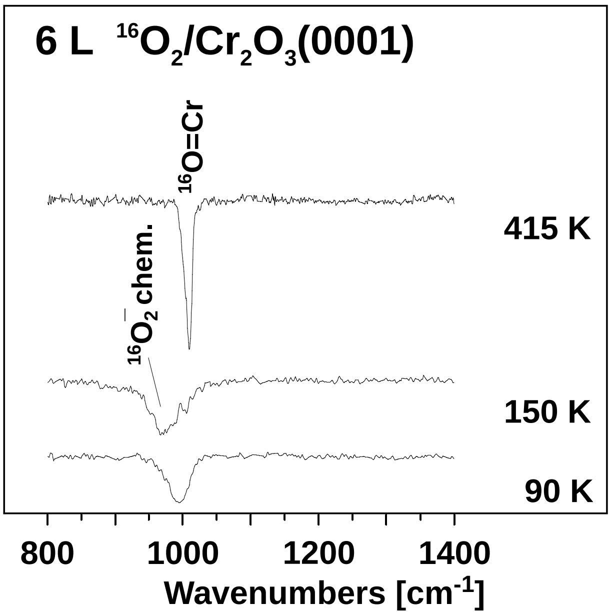

Figure 5. IRAS spectra after adsorption of a saturation coverage of O_2 on $Cr_2O_3(0001)/Cr(110)$. The spectra are taken at the temperatures indicated.

adsorption geometry [38]. Recent cluster calculations by Staemmler's group have revealed the reason for this [39]. The CO molecule is situated between two adjacent Cr ions. This allows the carbon lone pair to interact with the positively charged Cr ions and to reduce, simultaneously, the Pauli repulsion between the CO 1π electrons and the oxygen ions by placing the molecules atop an open oxygen triangle. This leads to a more stable adsorption than by placing the molecule vertically atop a chromium ion. However, the energy differences are only of the order of a few kJ so that it is fair to assume that the molecule is rather dynamic on the surface. It is very interesting to note that CO adsorption on $V_2O_3(0001)$ seems to show very much related behavior although the study of orientation of the molecule is not complete yet [27].

Another interesting case is CO_2 adsorption on solid surfaces. Wyn Roberts and his group have pioneered this field on metal surfaces [18, 40, 41]. Together with one of the authors he reviewed the field recently [42]. Here we report on the interesting case of CO_2 adsorption on $Cr_2O_3(0001)$ [43]. The adsorption can be almost completely suppressed when the $Cr_2O_3(0001)$ surface is oxygen terminated with chromyl groups. On the metal terminated surface, on the other hand, CO_2 is relatively strongly chemisorbed. The CO_2 molecule forms a carboxyl species bound through the carbon atom to a chromium ion. Interestingly, carbonates are only easily formed when promoters such as alkali metals are present.

METAL AGGREGATES ON OXIDE SURFACES: MORPHOLOGY, GROWTH AND ELECTRONIC STRUCTURE

So far, we have considered the clean oxide surface and its reactivity. In the following we will discuss the modification of the oxide surface by deposition of metal [3, 4]. The systems prepared in this way can be regarded as model systems in heterogeneous catalysis [4, 9]. They aim at bridging the so-called materials gap. Several groups have started to prepare such systems including Goodman [5], Henry [6], Madey [7], Møller [44] and our own group [2-4, 9]. The pioneer in this field was Helmut Poppa [45] who undertook the first systematic study applying transmission electron microscopy.

Figure 6 shows STM topographs of a clean alumina film (left), after deposition of Pd at room temperature on the clean film (middle) and onto a chemically modified film which is terminated by hydroxyl groups (right) [4] which can be identified via vibrational spectroscopy [46].

The surface of the clean film (left) is well ordered and there are several kinds of defects present: The lines represent line defects due to anti-phase domain boundaries [47]. We know from nucleation studies that there are about 1×10^{13} point defects per cm^2 present as well [3]. Pd deposited at room temperature leads to aggregates residing on the domain boundaries and steps (middle). The surface of these aggregates can be imaged with atomic resolution, showing that the aggregates are crystalline and terminated by (111) and much smaller (100) facets [48, 49]. The mobility of Pd under these conditions is high enough to allow nucleation at the stronger interacting line defects, whereas at 90 K the point defects determine the growth behavior. At this temperature we find aggregates statistically distributed across the entire surface of the sample.

If we deposit the same amount of Pd at room temperature onto the hydroxylated film as onto the pristine film, the dispersion of aggregates is by about an order of magnitude higher as shown in the right panel of Fig.

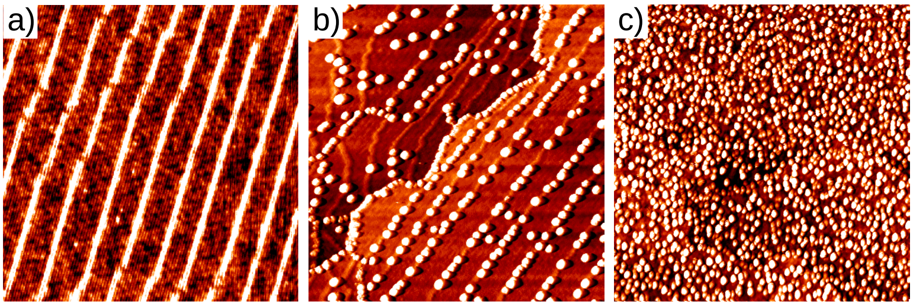

Figure 6. Scanning tunneling images (1000 × 1000 Å). a) Clean Al_2O_3/NiAl(100) film, U = 4.2 V, I = 0.5 nA. b) After deposition of Pd(0.2 Å) at 300 K, U = 3.1 V, I = 0.5 nA. c) After deposition of Pd (0.2 Å) at 300 K on a hydroxylated alumina film, U = 3.1 V, I = 0.4 nA.

6 [46]. This is due to stronger interaction with the substrate which also leads to higher thermal stability before agglomeration starts.

Studying this agglomeration process is an interesting subject in itself and research in this direction is only starting. A more basic aspect, of course, would be a study of metal atom diffusion on oxide surfaces. The obvious method to perform such a study is scanning tunneling microscopy. However, in contrast to diffusion studies on metal surfaces, similar studies on oxide surfaces have not been reported. On the other hand, field ion microscopy is being used in our group to study such processes. Applying neon-FIM at 79 K the feasibility to image platinum adatoms, supported on a thin alumina film grown on a [110]-oriented NiAl tip, had been demonstrated in our group [48]. At these conditions, the imaging of an *ensemble* of Pt adatoms is

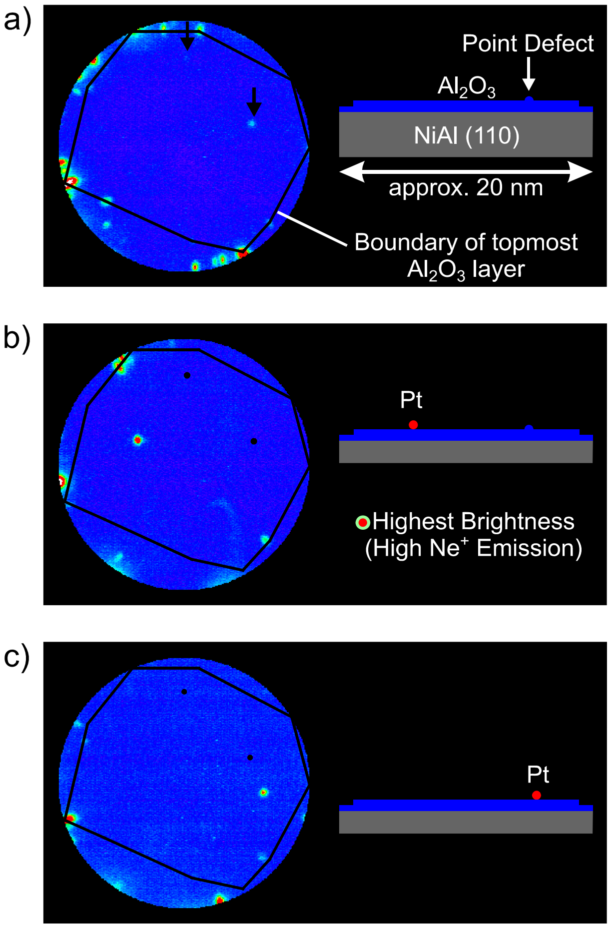

Figure 7. Surface diffusion of Pt/Al_2O_3/NiAl(110). The polygon curves had been drawn in the circular sections of the FIM-pattern to indicate the boundary of the topmost Al_2O_3 layer: a) before deposition; b) After deposition, an individual Pt adatom was imaged at 35 K using neon-FIM at 7.7 kV (black dots: positions of defects); c) After heating the surface to 170 K during 20 s at zero field.

characterized by strong fluctuations and non-optimum contrast, partly compensated by computer aided image processing. Intending to observe cluster formation, the oxide surface had been exposed to a relative high platinum dose followed by several heating cycles. As a result, a local ordering of platinum adatoms was obtained in the vicinity of a point defect; the arrangement of adatoms was compatible with the surface unit cell [48]. From a displacement analysis of the platinum adatom ensemble only a rough estimation of the diffusion activation energy was obtained. Recently, we have prepared an *individual* Pt adatom on the apex plane of an oxidized [110]-oriented NiAl tip using neon FIM at 35 K [50]. A sequence of FIM patterns obtained in a first, exploratory experiment is shown in Fig. 7. Circular sections of FIM images show the specimen surface after oxidation. Before deposition of platinum the Al_2O_3 film was imaged allowing to visualize sites at the boundary and point defects as in Fig. 7(a). After exposing the surface (at 35 K) to a platinum beam, a new emission site appeared which was interpreted as the image spot of a single platinum adatom.

Figure 8 gives a survey of exploratory examinations of the surface diffusion behavior for alumina-supported, individual platinum adatoms, based on FIM patterns such as in Fig. 7(b) and (c). At 160 K the Pt adatom is in fact more mobile on the well ordered oxide film than on NiAl(110) [50]. The onset temperature for surface diffusion was especially examined in another experiment (Fig. 9), allowing to estimate a value for the activation energy [51]. The identity of the adatom, prepared in the center of the plane was ascertained before and after the diffusion steps. In particular, upon the first heating step to 100 K for 15 s, the adatom changed its position slightly, but noticeably. In this case, our analysis of the jump direction is compatible with the model visualized in Fig. 10 [52].

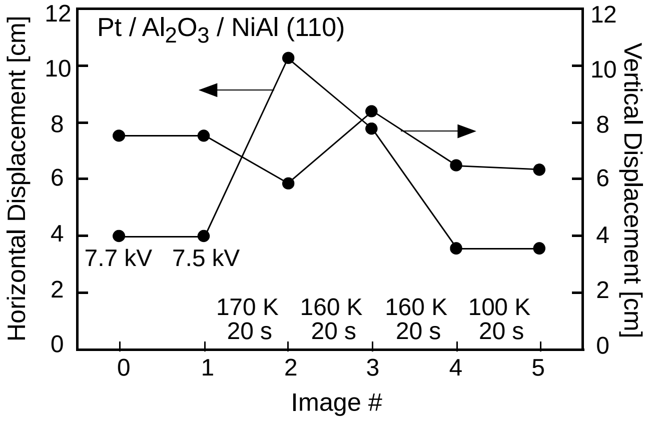

Figure 8. Positions of image spots of Pt adatoms diffusing on Al_2O_3/NiAl(110): Between the imaging cycles the temperature was varied from 170 K (Fig. 7c) to 100 K.

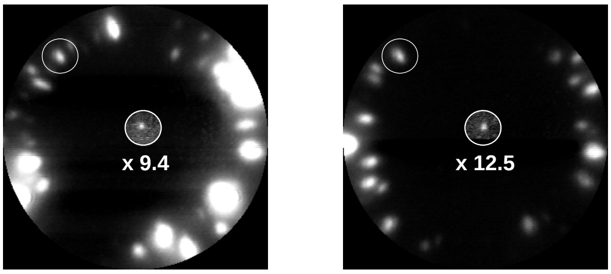

Figure 9. Onset of surface diffusion of a Pt adatom adsorbed in the center of an alumina film on NiAl(110): To improve the visibility, the intensity around the image spot of the adatom was multiplied by a factor 9.4 (a) and 12.5 (b). Image b) was taken after 15 s heating at 100 K without applied field. The circle at eleven o'clock marks the position of a step site serving as a reference at the boundary.

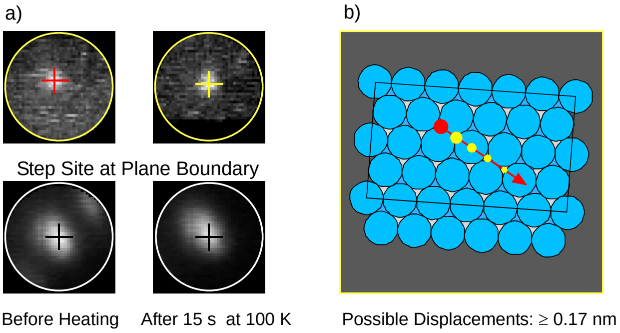

Figure 10. Onset of surface diffusion: a) experiment and b) model. Upper two enlarged FIM images in a) show positions of Pt adsorbed in the center of the alumina film prepared on NiAl(110) (Fig. 9). The lower two patterns display step sites whose image positions do not change upon heating. The model b) shows a simplified, hexagonal arrangement of the top layer of oxygen ions and the surface unit cell. The thick, red dot marks the position of the Pt adatom prior to heating. The yellow dots show possible positions after the diffusion event. The maximum displacement is estimated to approximately 0.5 nm considered though decreasing diameter of yellow dots.

In Table 1, we have compiled experimental and theoretical results of surface diffusion parameter for individual Pt adatoms. Those deposited on a thin alumina film supported on NiAl(110) showed an onset temperature for approaching 100 K. We note that our experimental estimate is probably close to 0.3 eV and thus significantly smaller than the calculated value, 0.7 eV obtained for Pt/Al_2O_3/Al(111) [53]. Though further experiments are still required, we conclude that the activation energy of Pt on a defect free surface area of Al_2O_3 is comparable with results of Pt surface diffusion on closely packed metal surfaces such as Ni(111) and Pt(111) [51]. The relatively high mobility at temperatures approaching 100 K is also in general agreement with previous STM investigations on Pt cluster formation occurring at low temperatures on alumina [3]. It is clear, however, that the characterization of the surface diffusion behavior of alumina-supported platinum requires more displacement observations.

Table 1. Surface diffusion parameter for individual Pt adatoms [50].

System	Onset Temperature (K)	Activation Energy (eV)
Pt/NiAl(110)	165	0.48
Pt/Ni(111)		<0.22 [51]
Pt/Al_2O_3/NiAl(110)	>100	>0.29
	<160	<0.47
Pt/Al_2O_3/Al(111)		0.7 [53]

It is obvious that the area of diffusion studies will considerably profit from atomic resolution, once it is obtained routinely for deposited aggregates on oxide surfaces. While for TiO_2 and very few other oxide substrates atomic resolution may be obtained routinely, there are very few studies on deposited metal particles where atomic resolution has been reported [49], [54]. The first report for an atomically resolved image of a Pd metal cluster on MoS_2 was reported by Claude Henry and his group [54]. A joint effort between Fleming Besenbacher and our group [49] has led to atomically resolved images of Pd aggregates deposited on a thin alumina film. Figure 11 shows such an image of an aggregate of about 80 Å in width. The particle is obviously crystalline and exposes on its top facet the (111) Pd surface. Also, the (111) facets on the side, typical for a cuboctahedral particle, can be discerned. The small (100) facets predicted via equilibrium shape considerations on the basis of the Wulff-construction could not be atomically resolved. If we, however, apply the concept of the Wulff-construction, we may deduce the metal surface interaction energy [49]. The basic equation is

eq. (1) $$W_{adh} = \gamma_{oxide} + \gamma_{metal} - \gamma_{interface}$$

Provided the surface energies (γ_{metal}) of the various crystallographic planes of the metal are known [55], a relative work of adhesion (W_{adh}) may

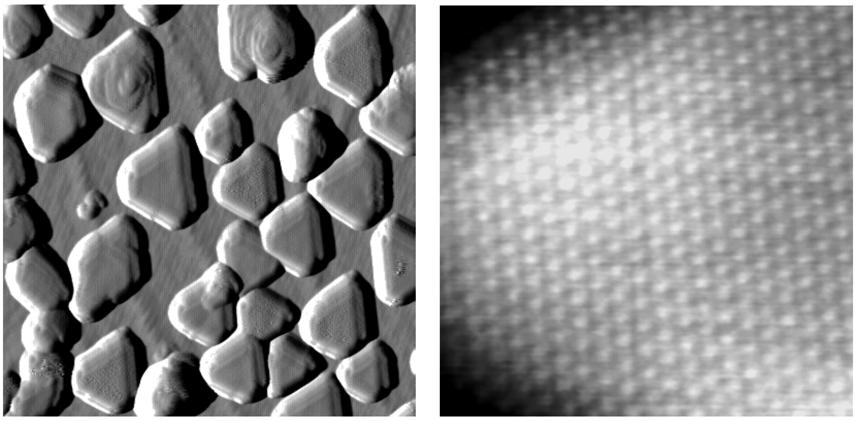

Figure 11. Scanning tunneling images at atomic resolution of Pd aggregates grown on an alumina film (left 500 × 500 Å, right 50 × 50 Å) [49].

be defined [49]. We find 2.9 ± 0.2 J/m^2 which is still rather different with respect to recent calculations by Jennison et al. [53] where metal adsorption energies (1.05 J/m^2) have been calculated on a defect free thin alumina film. It is not unlikely that this discrepancy is connected with the rather complicated nucleation and growth behavior of the aggregates involving defects in the substrate [56].

It is clear that these studies only represent a beginning, but we think they are promising. Parallel to studying morphology, structure and processes of cluster formation, we have investigated the electronic structure of deposited metal aggregates. In earlier studies we have used photoelectron spectroscopy and X-ray absorption to investigate deposits with finite but narrow size distributions to probe the size dependent electronic structure of these systems [56]. With the advent of scanning tunneling microscopy it has become possible to investigate individual objects, and therefore the spectroscopy of optical and electronic properties of single, selected objects on a surface has been in the focus of interest in recent years. It opens the unique possibility to detect local variations in the electronic structure which are normally hidden in the inhomogeneous broadening of the spectra due to statistical disorder on the surface. A local measurement allows the direct connection between a distinct geometric structure and its optical, electronic or chemical properties. In this way, the opening of a size dependent band gap has been observed in small Pt clusters with scanning tunneling spectroscopy [57]. The catalytic activity of small Au clusters has been correlated with the appearance of the metal non-metal transition as cluster sizes decrease [58]. Spectroscopy of single molecules in the STM has demonstrated the great potential of investigating molecular vibrations as a function of adsorption site [59]. With the first observation of light emission from the tunnel junction of a STM, the detection of optical properties of a surface with nanometer resolution has become feasible [60]. The method has been employed to measure photon maps of metal and semiconductor surfaces, nanocrystals and individual molecules [61]. The spectroscopy of emitted photons provides an insight in the underlying elementary processes, whereby tip-induced plasmon resonances have been identified as the source of the observed photon emission [61]. These special interfacial modes are connected with the strong electromagnetic interaction between the tip and the sample in a STM and are not visible in conventional optical spectroscopy. On the other side, typical features accessible to classical absorption spectroscopy, like Mie resonances in small metal particles or electronic transitions in molecules, have not been observed in the photon emission spectra from a tunnel junction of a STM. Therefore, there is still a gap to be bridged between conventional optical spectroscopy averaging over a macroscopic area of the surface and the emission spectroscopy in the STM at high spatial resolution. Here we report on photon emission from individual, alumina-supported Ag clusters [62]. The emission can clearly be distinguished from tip-induced plasmon modes and is interpreted as a decay of Mie-plasmon excitations in small metal particles, well known from absorption spectroscopy [63]. We have determined the Mie-plasmon energy and its homogeneous line width for single Ag particles as a function of cluster diameter between 1.5-12 nm.

In the experiment the tunnel tip of a beetle type STM, mounted in an UHV chamber, has been used as a local electron emitter. The electron energy could be adjusted in a wide range between 1-100 eV, the typical electron current was set to 1-10 nA. The electron injection from the tip caused electronic excitations in the sample followed by optical de-excitation processes. The emitted photons have been collected by a parabolic mirror surrounding the STM. Outside the vacuum chamber the light was focused onto the entrance slit of a grating spectrograph and detected with a liquid-nitrogen cooled CCD-camera. The spatial resolution of the emission spectroscopy depends on the tip-sample separation and therefore on the bias voltage applied. For tunnel voltages below 15 V the exciting electron current is restricted to an area smaller than 1.5 nm in diameter. Ag clusters were grown by vapor deposition at 300 K onto a thin, well-ordered alumina film prepared on a NiAl(110) single crystal [3]. The density of nucleation centers for the particles was controlled in a sputter-assisted deposition process. Depending on the amount of evaporated material the mean cluster size could be adjusted between 1-12 nm. The cluster diameter was determined after separating the effect of tip convolution. This was achieved by extracting a mean tip radius from the apparent broadening of step edges of the substrate.

The photon emission characteristics of a cluster-covered alumina film on NiAl(110) can be divided in two different excitation regimes depending on the tip voltage:

(1) Spectra measured at low tunnel voltages ($U_{tip} \leq 5$ V) are dominated by two emission peaks at 1.3 eV and 2.4 eV, which are almost independent of polarity (Fig.12, curve (i)). The emission is caused by collective electron oscillations in the coupled electron gases of tip and sample induced by a strong dynamic electromagnetic field in the tunnel cavity. Inelastically tunneling electrons are the driving force for these tip-induced plasmons [61]. The shape of the spectra is mainly determined by the dielectric function of NiAl. It can be reproduced within a theoretical model, which allows to calculate the electromagnetic response function of a simplified tip-sample geometry, using the dielectric function of the W tip and the NiAl sample as material properties [64]. The thin alumina film and the presence of small metal clusters below the tunnel tip slightly modify the shape and intensity of the spectra emitted from the clean NiAl/W tunnel junction.

(2) An increasing tunnel bias gradually decreases the tip-sample interaction and consequently the photon yield due to inelastic tunneling processes. At voltages above 10 V the characteristic lines of the tip-induced plasmon vanish. In contrast to the clean alumina surface, a new, intense emission line appears in the spectra taken on top of an Ag cluster (Fig.12,

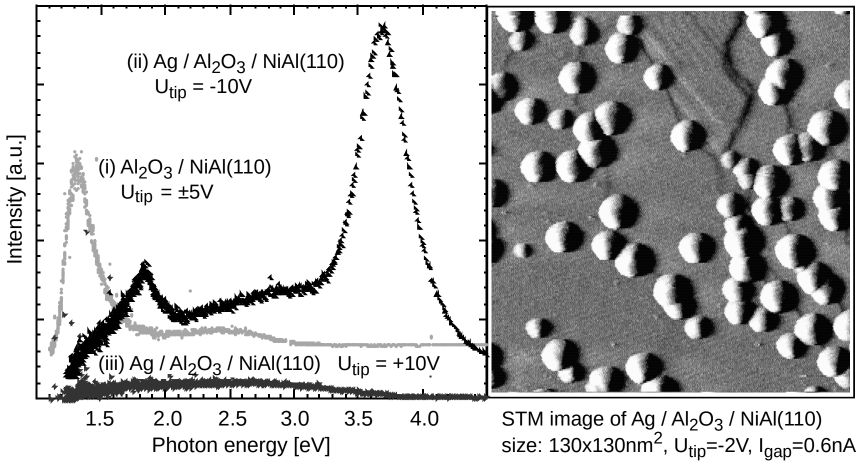

STM image of Ag / Al_2O_3 / NiAl(110)
size: 130x130nm^2, U_{tip}=-2V, I_{gap}=0.6nA

Figure 12. Photon emission spectra at different tip voltages and STM image of $Ag/Al_2O_3/NiAl(110)$.

curve (ii)). The peak is centered around 3.7 eV and visible only for the injection of electrons from the tip into the cluster (see curve (iii) for comparison). The energetic position of the emission line corresponds to the 1,0-mode of the Mie plasmon, well known from extinction cross section measurements on Ag cluster ensembles [63]. The resonance is interpreted as an oscillation of the free silver electron-gas perpendicular to the substrate plane. The corresponding in plane oscillation (1,1-mode) is not accessible to the experiment because the incoming electrons from the tip induce preferentially a dipole or impact excitation along the surface normal. Additionally, the 1,1-mode is strongly damped by its image dipole induced in the NiAl substrate. For a detailed discussion see ref. [62].

The energy position and the line width of the Mie plasmon show a characteristic dependence on cluster size [62](see Fig.13). For decreasing cluster diameter from 12.0 to 1.5 nm a blue shift of the plasmon energy from 3.6 eV to almost 4.0 eV is observed. In the same size range the homogeneous line width of the emission increases from 160 meV to 300 meV. Both size dependencies show an 1/d (d = cluster diameter) behavior reflecting the growing surface contribution with respect to bulk effects in small particles. For the blue shift of the peak position changes of the intrinsic electronic properties in a spatially confined system are considered. In the case of Ag particles the plasmon energy is determined by the classical Drude frequency of the free 5s electrons drastically reduced by a strong screening effect of the 4d electrons [65]. The 4d depolarization field vanishes at the cluster surface because the 4d electrons are more localized at the Ag atoms and have a low residence probability outside the classical cluster volume. In contrast, a fraction of the Ag 5s electrons spills out into the vacuum, where they are unaffected by the 4d screening and increase their plasmon frequency. With decreasing cluster size this fraction of free

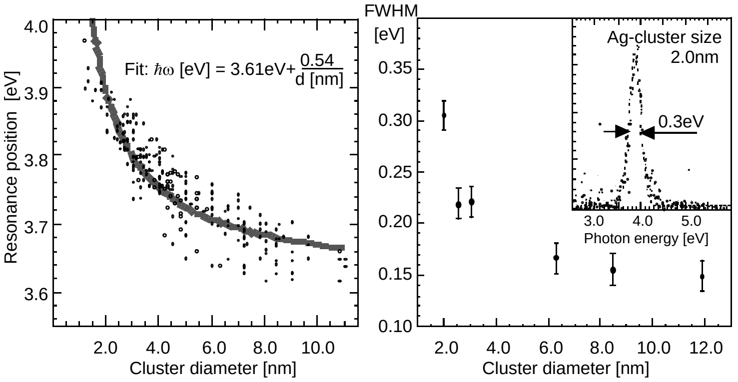

Figure 13. Energetic position and line width of the Mie resonance as a function of cluster diameter.

electrons residing outside the classical cluster volume increases with respect to the total electron number and the Mie plasmon energy shifts to higher energies. This effect is partly cancelled, because a considerable electron spill out results also in a reduction of the electron density inside the cluster volume and thus a red shift of the plasmon energy with decreasing cluster size ($\omega_{plas}^2 \sim n_{electron}$). However, in the present experiment the electron spill out is strongly quenched at the cluster-alumina interface and the blue shift dominates the size dependence of the Mie plasmon. A quantitative description of the experimental results has to treat the 5s-4d interaction on a fully quantum-mechanical level and has to include the restructuring of the bulk electronic structure in small Ag particles.

For the increase of the homogeneous line width of the Mie resonance with decreasing cluster size, only an empirical model can be presented as well. The behavior reflects the reduced lifetime of the collective electron oscillation in small particles due to an enhanced electron-surface scattering rate. This additional decay mechanism (apart from electron-electron, electron-phonon scattering and Landau damping) becomes highly efficient, when the electron mean free path exceeds the cluster diameter and causes a dephasing process of the collective oscillation [63]. The surface mediated character of the damping with respect to the cluster volume can explain the observed 1/d behavior of the line width with decreasing cluster size.

MAGNETIC PROPERTIES

In addition to investigations on electronic properties it is interesting to develop tools which allow us to study magnetic properties. Based upon the experience we have developed using electron spin resonance (ESR) on radicals adsorbed on single crystal surfaces [66-68] we have started measurements of the ferromagnetic resonance (FMR) [69, 70] of deposited

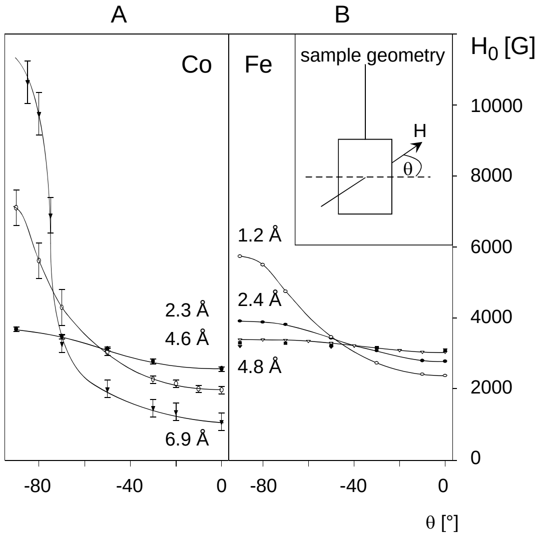

Figure 14. Angular dependence of the resonance field for various amounts of Co (A) and Fe (B) deposited at room temperature on an Al_2O_3(0001)-single crystal surface. θ denotes the angle between the crystal surface and the static magnetic field. The deposited amounts are given in terms of the effective layer thickness.

aggregates. To this end we prepare either a bulk single crystal oxide surface or an epitaxial thin oxide film under ultrahigh vacuum conditions and grow the metal aggregates on it. Such a sample is brought into a microwave cavity and the FMR is recorded. The sample, which is attached to a manipulator may be oriented with respect to the external field, and therefore the orientation of the direction of the magnetization is accessible.

Figure 14a shows such a measurement for Co particles on Al_2O_3(0001), deposited at room temperature. An uniaxial orientation is found with a single minimum at orientation of the field parallel to the surface plane. This means that the magnetization is also oriented in this way [70]. A very similar behavior is found for iron as plotted in Fig. 14b. The smaller asymmetry is a property of the specific metal. While upon heating the behavior does not change for Co, it becomes more complex for Fe (see Fig. 15) [71].

This is indicative for the survival of uniaxial magnetism in the hexagonal cobalt and its breakdown for the body centered cubic iron. Fe(bcc) has three easy axes of magnetization and the formation of more crystalline aggregates is likely to be the reason for the observation.

Since atomic resolution is very hard to achieve on the small aggregate at present, these experimental observations in the ferromagnetic resonance are very useful. FMR can also be used to follow adsorption of the aggregates. We find that chemisorption of CO quenches the surface magnetism of the small particles. Oxidation of the small particles leads to the formation of an oxide skin on a ferromagnetic kernel. Since the oxide signal occurs at very different fields only the FMR of the kernel has been recorded. Such measurements may be used to follow the formation of oxide aggregates

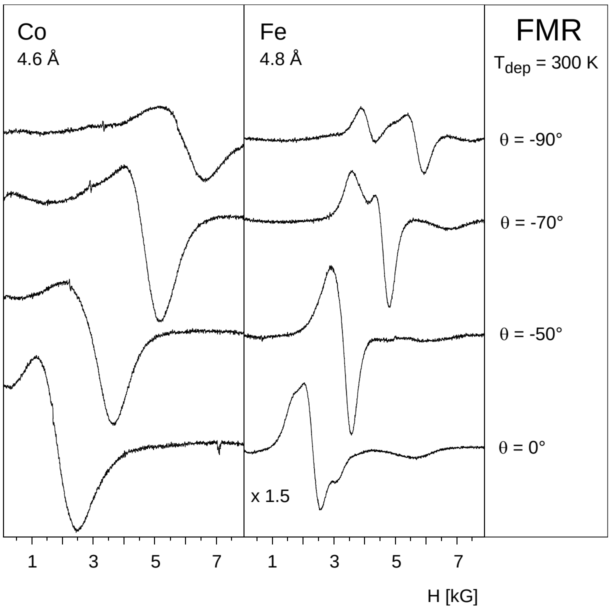

Figure 15. Comparison of the angular dependent FMR-spectra of Co and Fe on $Al_2O_3(0001)$ after heating the deposits (prepared at 300 K) to 870 K. The spectra were recorded at 300 K. θ denotes the angle between the static magnetic field and the crystal surface. The deposited amounts are given in terms of the effective layer thickness.

deposited on oxide supports which would have interesting catalytic properties.

ADSORPTION AND REACTION

It is the next step to investigate adsorption and reaction of molecules on the surfaces of the deposited metal aggregates. Several groups have used Fourier Transform Infrared (FTIR) spectroscopy to study adsorption on such systems [72]. The results have been published and discussed in several review articles [3, 72]. Here we describe and discuss possibilities that arise from a combination of molecular beam studies in direct combination with a fast FTIR spectrometer where in-situ studies are possible [73, 74].

The experiments have been performed in a new UHV molecular beam / surface spectroscopy apparatus. It has been specifically designed for kinetic studies on complex model systems.

After preparation the sample is transferred to the scattering chamber, which contains an experimental setup as depicted schematically in Fig. 16. Up to three molecular beams can be crossed on the sample surface providing the reactants. In kinetic studies requiring high reactant fluxes two modulated effusive sources can be used, for sticking coefficient measurements or angular resolved scattering a third beam with narrow velocity distribution and well-shaped profile is generated from a supersonic source. Angular-

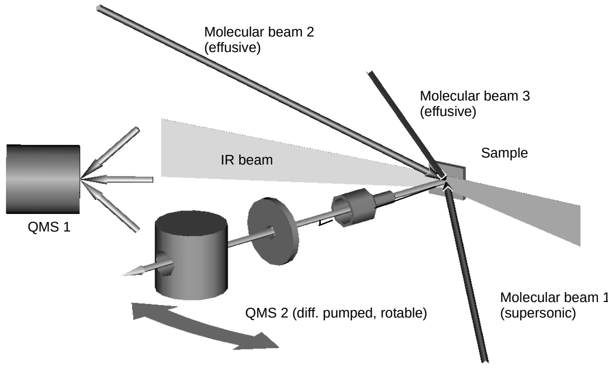

Figure 16. Schematic representation of the molecular beam/IR spectroscopy experiment.

integrated gas-phase measurements are performed with a quadrupole mass spectrometer, angular-resolved measurements with a second rotatable and doubly differentially pumped QMS. Simultaneously, time-resolved IR absorption spectra can be obtained via a vacuum FT-IR spectrometer. A detailed description of the experimental setup and data acquisition procedure can be found elsewhere [74].

One general effect which has to be taken into account in a description of the adsorption or reaction kinetics on supported metal catalysts is *support mediated adsorption* (sometimes also denoted as *reverse spillover*). The process is schematically illustrated in Fig. 17d: An impinging gas molecule may directly collide with the Pd particle and adsorb with a probability given by the sticking coefficient on Pd. Alternatively, the molecule may impinge on the substrate, be trapped in a physisorbed state and reach the metal particle via surface diffusion (this established a “capture zone” for the particle). Depending on the diffusion length, this effect may considerably enhance the adsorbate flux to the metal particle and has to be taken into consideration when comparing catalytic activities. Gillet et al. [75] have formulated the effect for CO adsorption on Pd particles. Later it was taken into account in several adsorption and reaction studies on the same system [76-78]. Models have been derived, which allow support diffusion to be taken into account quantitatively in kinetic studies [79-82].

Combining structural information with molecular beam experiments, a possible contribution to adsorption due to support trapping can be easily quantified. The procedure is illustrated in the example shown in Fig. 17. First, we determine the net sticking coefficient for the model system (Fig. 17c) via a King and Wells type sticking coefficient measurement [83, 84]. Taking into account the fraction of the support, covered by the active metal (from structure studies, [3, 85, 86]) and the sticking coefficient on the clean metal surface (from single crystal data, [87]) the support trapping contribution can be directly estimated. In order to quantify a ‘capture zone’ (an average area from which an adsorbate diffuses to the metal particle), however, we have to take into account that only a certain fraction of the

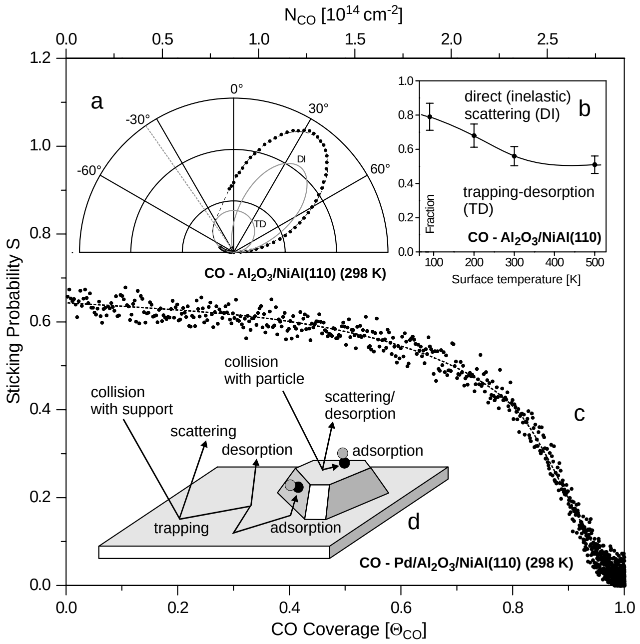

Figure 17. (a) Angular distribution of CO (kinetic energy 86 meV, incidence angle: -35°) scattered from Al_2O_3/NiAl(110); (b) Trapping-desorption and direct inelastic scattering components for CO scattered from Al_2O_3/NiAl(110) as a function of surface temperature; (c) Sticking probability for CO on Pd/Al_2O_3/NiAl(110); (d) Schematic representation of the process.

adsorbate molecules is initially trapped in a physisorption well on the oxide surface (trapping-desorption channel, TD), while the remaining molecules are directly scattered back into the vacuum (direct inelastic scattering, DI).

The probabilities for both processes can be derived from angular and/or time resolved scattering studies from the free support surface (Fig. 17a): The directly scattered molecules are characterized by an angular distribution centered around the specular direction and a velocity distribution dependent on the incident beam. The trapped adsorbates exhibit a symmetric distribution with respect to the surface normal (the information on the initial impulse is lost upon accommodation) and a velocity which depends on the surface temperature (in practice the situation might be complicated by partial accommodation, inefficient coupling of parallel and perpendicular momentum [88, 89] or due to diffuse scattering from defects, see e.g. [6]). As an example we show the corresponding measurements for CO adsorption at 300 K on the alumina-supported Pd model catalyst (Fig. 17). Under these conditions it is found that the support-trapping represents the dominating adsorption channel, as the ‘capture zone’ of the Pd particles exceeds the particle distance [90]. With increasing surface temperature, the diffusion length on the support decreases and eventually, depending on the strength of the adsorbate-support interaction, the support-trapping effect is expected to become less important.

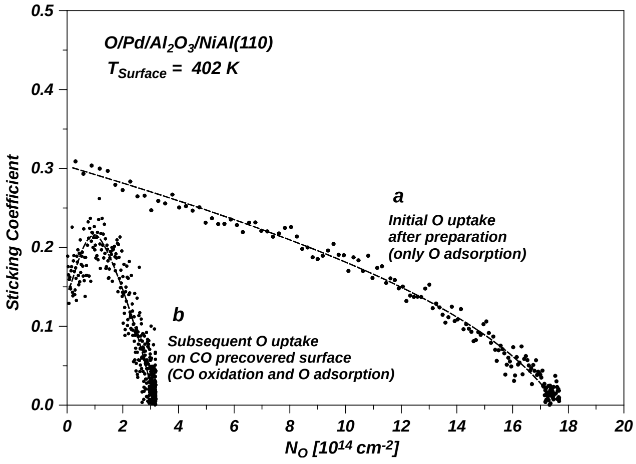

Figure 18. Oxygen sticking coefficient as a function of oxygen uptake (in O atoms/cm^2) at 402 K for Pd particles supported on Al_2O_3/NiAl(110) directly after preparation under UHV conditions and after several cycles of O_2 and CO exposure.

The interaction of oxygen with Pd surfaces as well as the formation and influence of subsurface and bulk oxygen is a controversially discussed topic (see e.g. [76, 87, 91-111] and refs. therein). The remaining ambiguities, which exist in spite of the numerous studies published, are mainly related to the difficulties in the identification of bulk and subsurface oxygen species, the lack of quantitative adsorption and reactivity studies and the limited knowledge about the surface defect structure. Here, we may again take advantage of the quantitative character of molecular beam experiments, as will briefly be illustrated in this section. A more detailed discussion of the topic can be found elsewhere [73].

In CO oxidation experiments, there have been indications that even at low sample temperatures and oxygen exposures, rapid subsurface or bulk diffusion of adsorbed oxygen may occur [73]. In order to test this hypothesis, we have performed O_2 sticking coefficient measurements in a temperature range from 100 to 400 K. An example is depicted in Fig. 18, where we compare the sticking coefficient displayed as a function of oxygen uptake for two situations, (a) the freshly prepared Pd sample (Fig. 18a) and (b) after repeated cycles of O_2 and CO exposure (Fig.18b). Considering the situation after repeated O_2 and CO exposure, the total oxygen uptake can be subdivided into a reactive contribution due to oxidation of the preadsorbed CO and adsorptive contribution. Taking both into account, the adsorption uptake turns out to be consistent with what is expected for simple Pd(111)-like surface adsorption behavior based on the Pd surface area estimate from STM and high-resolution low energy electron diffraction LEED [73].

If we compare this result with the oxygen sticking diagram for the Pd particles initially after preparation (Fig. 18a), we find a much larger oxygen uptake. These values are by far too large to be compatible with pure surface adsorption. Therefore, we have indeed to take into account rapid surface and bulk diffusion on the time-scale of the experiment. Moreover, the reduced oxygen uptake after subsequent CO and O_2 exposure shows that the bulk oxygen species are not accessible to the CO oxidation in this temperature region. This observation is in agreement with a recent study on Pd(111) [106].

Next, we may consider the total oxygen uptake detectable in sticking coefficient measurements as a function of the substrate temperature (Fig. 19). Initially, we find a low and slowly decreasing uptake in the temperature range between 100 K and 250 K, followed by a step-like increase in the temperature regime ≥ 300 K. Based upon previous adsorption studies, we may differentiate between three adsorption regimes: (I) At temperatures around 100 K the adsorption process is molecular [96], before at higher sample temperatures O_2 will dissociate [96]. This process is connected to a decreasing saturation coverage [99]. The sudden increase in the uptake above 250 K marks the onset of bulk diffusion. Note that in contrast to adsorption experiment on bulk metal samples, the bulk reservoir saturates rapidly and the uptake becomes independent of the sample temperature. A simple estimate reveals that the total oxygen uptake upon saturation corresponds to a total stoichiometry of $PdO_{0.5\text{-}0.8}$. Beyond this saturation uptake, the net oxygen adsorption decreases below the detection level of the experiment.

Previously, it has been reported that supported Pd particles may undergo morphological changes induced by strongly interacting adsorbates [108]. Although the conditions are rather moderate in this work, we have performed STM measurements after bulk-O-saturation (i.e. after a repeated O_2 and CO treatment) in order to exclude such effects as a possible reason for the changes in adsorption behavior [73]. A comparison with the STM images taken before oxygen adsorption shows that neither the particle

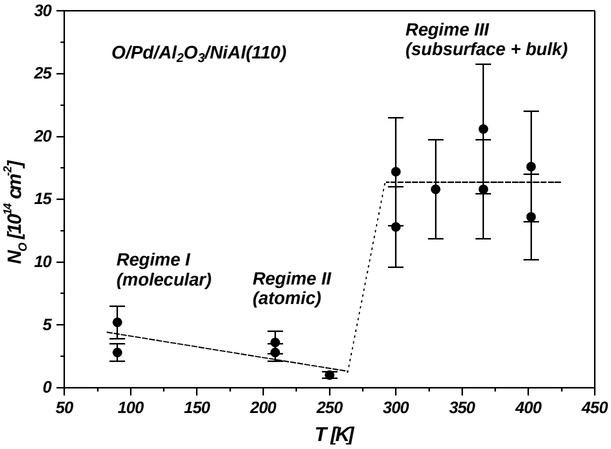

Figure 19. Oxygen uptake (in O atoms/cm^2) of a sample of Pd particles supported on Al_2O_3/NiAl(110) directly after preparation under UHV conditions as a function of the sample temperature.

density nor the overall morphology of the Pd aggregates is affected by the large oxygen uptake. Only slight distortions of the particle edges appear, which might be interpreted as an indication for a distortion of the Pd lattice structure due to the incorporated oxygen.

Thus, we may conclude that, starting at temperatures above 250 to 300 K, the Pd particles incorporate large amounts of oxygen on the time-scale of the sticking or reactivity experiments. In comparison, on single crystal surfaces this process is typically found to proceed significantly slower and is observed at higher temperatures ([106] and refs. therein). It has been suggested, however, that the kinetics of bulk diffusion may strongly depend on the defect density of the system [92, 94, 95]. This appears consistent with the present study, as in comparison with most single crystals, the supported Pd nanocrystallites in this work represent a high defect-density system. In addition to step and edge sites, we have to take into account the particle-oxide interface, where the crystallite structure may be additionally distorted due to interactions with the support. These effects may facilitate a drastically enhanced bulk diffusion for small particles, even in comparison with defective single crystal samples. Indeed, an anomalous large oxygen uptake at low temperature was previously observed for Pd supported on γ-alumina [76, 91], although in this study no exact morphological characterization of the particles was available and no systematic temperature dependence was reported.

In view of these results, it becomes evident that studying the kinetics of test reactions such as the CO oxidation on supported nanoparticles, we have to explicitly take into account the influence of bulk diffusion, even at low reaction temperatures.

After the discussion of the adsorption and interaction of the model systems with simple adsorbates we will now proceed to the CO oxidation as a simple model reaction. Using molecular beam methods, the reaction has been studied both on single crystal Pd surfaces [112-114] and on supported Pd particles [6, 76-78, 91].

As discussed elsewhere [73], a stable oxidation kinetics on the Pd particles is only obtained after saturation of the bulk oxygen reservoir. Therefore, we will consider the reaction kinetics on the fully oxygen saturated system, only. Again, we may take advantage of the single scattering conditions of the molecular beam experiment, which allow us to perform a simultaneous measurement of the reactant sticking coefficients and the CO_2 production rate. An example is displayed in Fig. 20, where the oxygen precovered surface was exposed to the CO beam. From a simultaneous measurement of the CO sticking coefficient (Fig. 20b) and the CO_2 production rate (Fig. 20a), the CO and oxygen coverages (Fig. 20c) as well as the absolute reaction rate (Fig. 20d) and eventually the apparent Langmuir-Hinshelwood (LH) rate constant (Fig. 20d) can be determined in a straightforward manner. A detailed description of the procedure can be found in the literature [76, 90, 91, 112]. From a series of similar measurements at different temperatures between 350 and 450 K, the activation barrier for the LH step as a function of oxygen or CO coverage is determined. In the limiting case of high oxygen and low CO coverage we derive an activation barrier of 57 ± 8 kJ mol^{-1}. For the reverse experiment, i.e. exposing a CO precovered sample to an oxygen beam, we obtain an activation barrier of 62 ± 9 kJ mol^{-1} (limiting case of high CO and low oxygen coverage).

It has to be concluded that the present results do not confirm a reduced activation barrier for the small Pd particles as has been suggested previously [76, 91]. Moreover, it is noteworthy that the activation energies are in excellent agreement with the activation barrier determined in the low temperature and high oxygen coverage regime for Pd(111) [112, 113]. Although this may not have been explicitly checked in the mentioned study [112], we may anticipate that subsurface and bulk oxygen formation play a less important role in kinetic studies on the close packed Pd(111)

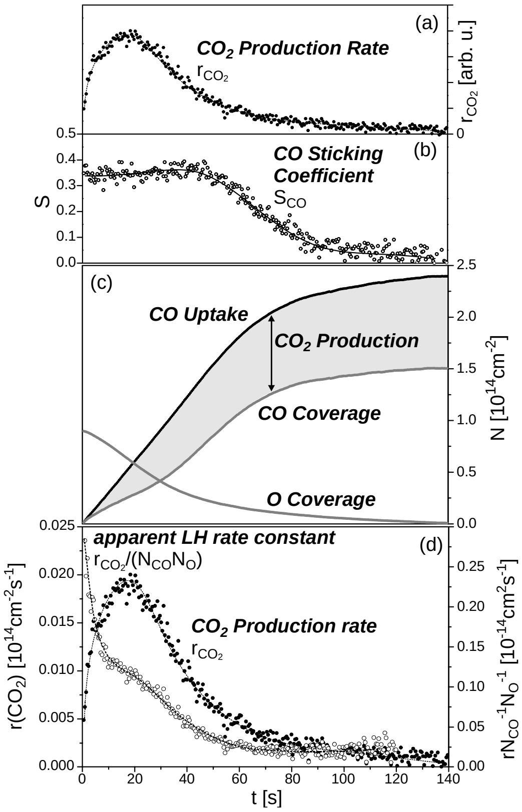

Figure 20. (a) Relative CO_2 production for oxygen-precovered Pd particles on Al_2O_3/NiAl(110) at a sample temperature of 402 K; (b) CO sticking coefficient as a function of experiment time; (c) O and CO surface coverages; (d) absolute CO_2 production rate and apparent Langmuir-Hinshelwood rate constant.

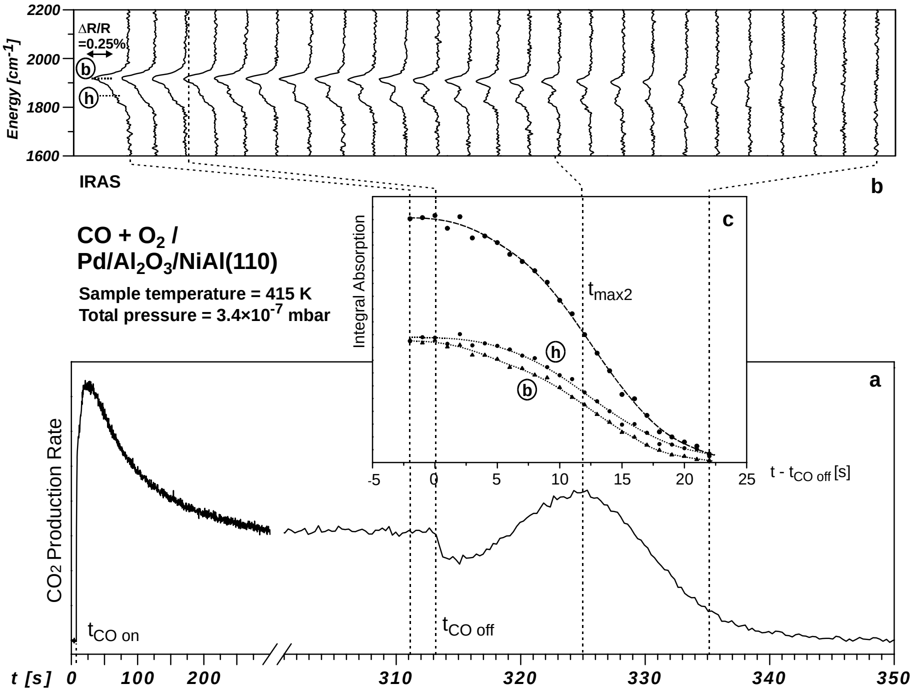

Figure 21. Simultaneous reactivity (a) and time-resolved IR reflection absorption spectroscopy experiment (b) during the transient region upon termination of the CO beam; (c) Integral absorption for the IRA spectra presented in (b) and partial absorption in the bridge (b) and hollow (h) regions.

surface. This, however, would mean that the large oxygen uptake of the Pd nanoparticles may only have a minor influence on the kinetics of the CO oxidation reaction. In future studies this conclusion will have to be tested employing experimental techniques which allow a direct and quantitative detection of subsurface oxygen species in combination with a well controlled variation of the structural parameters of the metal deposits.

Among the different kinetic effects, which may influence the reaction kinetics on supported catalysts, surface diffusion mediated coupling between different types of adsorption sites has recently attracted considerable attention [79-81]. The presence of different types of adsorption sites in close proximity is an intrinsic property of complex catalytic systems. Such types of adsorption sites may be e.g. different facets on nanocrystallites, step, edge or other defect sites, interface sites located at the particle boundary or adsorption sites on the support material itself. Recently, Zhdanov and Kasemo [115] have extensively reviewed simulations of such coupling processes. They have shown that relatively moderate changes in the sticking coefficients or reaction/adsorption energetics may drastically change the reaction rate under certain conditions. Still, the experimental verification of these effects is not straightforward and very few examples exist in the literature.

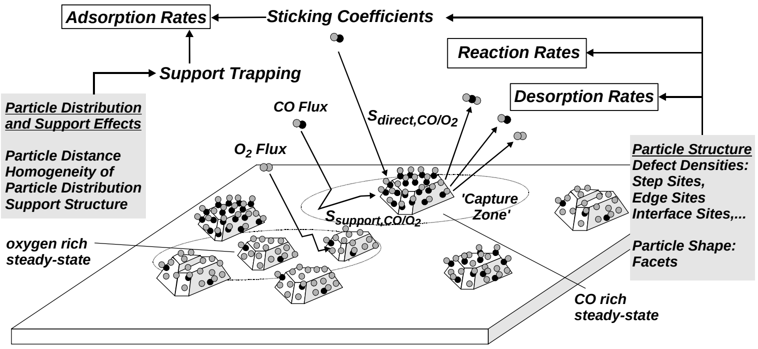

Figure 22. Schematic representation of the factors which may influence the individual adsorption and reaction behavior of the particles. Depending on their structure the steady-state adsorbate coverages of the particles may differ considerably, depending on the individual particle structure and surrounding.

Recently, Becker and Henry have observed a transient behavior in a beam experiment, which was related to an such heterogeneity effect [77, 78]: Upon termination of the CO flux for a system under steady-state reaction conditions, they observed a sudden decrease of the CO_2 production rate, followed by a smaller CO_2 production peak. Becker and Henry originally suggested an explanation which involves rapid desorption of CO from regular sites. CO adsorbed at defect sites, on the other hand, was assumed to be bound more strongly. Thus, these sites may remain fully saturated until the CO reservoir on the facets is largely depleted. Only after vacancies among these defect sites are generated, the reaction rate increases again, giving rise to the observed smaller maximum in the CO_2 production rate.

Since the Pd crystallites in this study are composed of similar facets ((111) and (100)), the effect is also expected for the present model system. Indeed, we find that under certain flux conditions we observe a transient CO_2 peak (Fig. 21a), which appears very similar to the effect originally reported [77, 78]. By performing a time-resolved FTIR experiment simultaneously with the reactivity measurement, however, it can be shown that the sudden decrease in the reactions rate is not related to spontaneous desorption of CO (Fig 21b). Moreover, the CO_2 peak intensity shows a continuous dependence on the CO flux, indicating that it is not likely to be related to defect sites. A more detailed discussion of this issue can be found elsewhere [116].

In contrast to the previously suggested explanation, experimental observations indicate that the effect, at least for the present supported model catalyst, is not related to a specific type of defect sites present on the Pd particles. A detailed discussion of the effects which instead may give rise to the observed behavior can be found in the literature [116]. Here, we would like to further discuss one particular contribution, which is related to the intrinsic heterogeneity of the system and thus is likely to be characteristic for most supported model catalysts: We have to take into account that every metal particle represents a largely isolated reaction system, in a sense that adsorbate diffusion from one particle to another is strongly suppressed (due to the weak adsorption on the support). Still, the reactant flux to the particle, the adsorption and the reaction rate for each individual particle may differ considerably. Possible reasons are variations in the adsorption rate due to a different overlapping of the 'capture zones' discussed above, as well as variations in the sticking coefficients, the desorption or reaction rate induced by differences in the individual particle structure (see schematic representation in Fig. 22).

As for the CO oxidation reaction the adsorbate surface coverage may sensitively depend on the adsorbate fluxes and reaction rates, a supported particle system may under steady-state conditions be in a 'mixed' state, i.e. with a fraction of the metal particles may be in an oxygen-rich and a fraction in a CO-rich reaction state. A superimposition of the transient behavior of both states may explain the observed effects [116].

It remains the question in how far these contributions can be included in further microkinetic simulations to finally yield a more complete picture of the reaction kinetics of the model system. On complex catalytic surfaces, on which naturally a certain degree of heterogeneity exists, such simulations will be a necessity in order to identify and quantify the kinetic effects under discussion. As a basis, this task, however, will require a detailed knowledge of the energetic and structural properties of the model system. Here, the available data are still rather limited. Whereas some detailed and representative structural information is available from STM and TEM (transmission electron microscopy), the data basis on gas-surface interaction and surface adsorption/reactions is largely limited to single-component systems and to ideal single crystal surfaces. Starting from these simple cases, studies on supported model catalysts with a reduced and controllable level of complexity may provide a way to address such questions.

In the preceding examples we have shown how metal nanoparticles adopt themselves to reaction conditions, induced by gases and/or high temperature. It is obvious that this effect has a strong influence on the adsorption and turnover of reactants. However, even if the catalyst surface is unaffected and behaves rigid and simply "waits" for the reaction to occur, the structure of an adsorbate under reaction conditions is probably still different from UHV experiments. At the high pressure of a catalytic reaction surface coverages may be obtained that can not be reproduced by the small exposures of surface science studies (typically on the order of Langmuirs, 10^{-6} Torr sec). If the "saturation" coverage of UHV experiments is exceeded, new adsorbate structures may form, as shown e.g. by a high pressure STM study of CO on Pt(111) [117]. Furthermore, at high pressure weakly adsorbed species are present with much higher concentration (resulting from a higher rate of adsorption) than under low pressure when they quickly desorb [118]. In the most unfavorable case, prominent species of low pressure studies may simply be spectators under high pressure conditions.

In order to tackle this problem a surface sensitive technique is needed that allows to monitor adsorbates under reaction conditions (~ 1 bar). A high pressure environment prevents the use of electron spectroscopies but is compatible with photon-based techniques such as infrared-visible sum frequency generation (SFG) spectroscopy. IR-vis SFG is a type of laser spectroscopy that is able to acquire vibrational spectra of adsorbates from UHV to ambient conditions. Due to its inherent surface sensitivity, surface vibrational spectra can be recorded even in the presence of a gas phase, in contrast to infrared reflection absorption spectroscopy (IRAS) that encounters problems with the excitation of rotational bands in the gas phase at pressures > 1 mbar, obstructing the surface species information. A detailed description of the SFG process can be found in the literature [118-121]. SFG is a second-order nonlinear optical process which involves the mixing of tunable infrared (ω_{IR}) and visible light (ω_{vis}) to produce a sum frequency output ($\omega_{SFG} = \omega_{IR} + \omega_{vis}$). The process is only allowed in a medium without inversion symmetry (in the electric dipole approximation), e.g. at surfaces where the inversion symmetry is broken. The dominant SFG signal is hence generated by the modes of the adsorbate, while the centrosymmetric bulk of face-centered cubic metals and an isotropic gas phase give nearly zero contribution to the SFG signal.

It was already mentioned in the introduction that single crystals can not fully represent supported metals. In order to include size and electronic effects, surface rearrangements, etc. in a pressure-dependent study of gas adsorption, SFG spectroscopy should be ideally carried out on supported nanoparticles. Although the applicability of SFG spectroscopy to nanostructured supported catalysts has been questioned for several reasons (scattering of laser beams on rough surfaces, disordered adsorbates, small total coverages), we recently succeeded to obtain SFG spectra from CO adsorbed on supported Pd nanoclusters [10]. Pd/Al_2O_3/NiAl(110) model catalysts were prepared as described above, and transferred under vacuum to a SFG-compatible UHV high pressure cell. Details about the sample preparation and cell design are published elsewhere [10, 119].

Figure 23 shows SFG spectra of CO adsorption on alumina supported Pd particles of 3 nm mean size (about 300 atoms per particle), grown at 90 K (particle density 10^{13}/cm^2). According to LEED and STM measurements [3, 122], the particle surface exhibits a high defect density as a result of the low growth temperature. Figure 23a displays SFG spectra taken at 190 K. Two peaks are clearly identified at 10^{-7} mbar CO and, according to IRAS results on Pd single crystals [123-125], they originate from bridge bonded CO at 1976 cm^{-1} and from terminal (on-top) CO at 2106 cm^{-1}. If one takes the integrated SFG signal intensity as a measure of the ratio of on-top to bridge-bonded CO, a value of about 0.5 is obtained. However, this value is only taken as an estimate here, since the SFG intensity can not be easily correlated with the concentration of a particular surface species. The

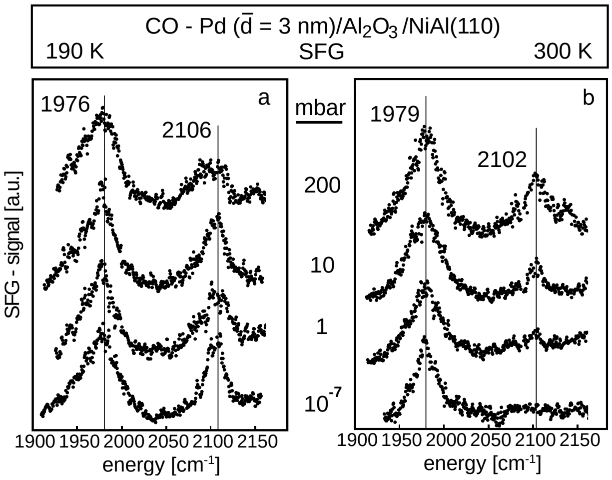

Figure 23. SFG spectra of CO adsorption on a Pd/Al_2O_3/NiAl(110) model catalyst at 190 K (a) and 300 K (b) (3 nm Pd particles grown at 90 K). The observed resonances are characteristic of bridge bonded CO and terminally bonded CO can be re-populated at ≥ 1 mbar.

coexistence of bridge and on-top bonded CO, a situation which is not found on Pd single crystals, reflects the defective structure of the Pd nanoparticles. In fact, the site occupancy on the Pd aggregates compares best with defect-rich single crystal Pd(111) or rough Pd thin films [123, 124, 126]. The difference between supported Pd aggregates and Pd(111) could result from a reduced lateral CO interaction on the nanoparticles or from the presence of additional crystal planes.

Increasing the pressure to 1, 10 and 200 mbar CO had only a small effect on the peak frequencies and also the ratio of on-top vs. bridge CO was nearly unchanged (Fig. 23a). If the sample temperature is raised to 300 K (Fig. 23b), which is above the desorption temperature of on-top CO on Pd clusters under UHV conditions [3], bridge-bonded CO is the only species that can be observed by SFG at 10^{-7} mbar. However, the on-top adsorption sites can be populated at $p \geq 1$ mbar, and at 200 mbar CO a relative on-top/bridge ratio of ~ 0.5 can be obtained, similar to the value at 190 K.

Comparing Figs. 23a and 23b illustrates the pressure- and temperature-dependent adsorption site occupancy of CO on Pd/Al_2O_3. While at 190 K an extrapolation of the 10^{-7} mbar spectrum to 200 mbar would lead to a satisfactory result, for a temperature of 300 K the prediction would be wrong (absence vs. presence of on-top CO). In addition, the adsorption site occupancy of Pd nanoparticles is influenced by the particle size and surface structure. If the same experiment is carried out on Pd particles grown at 300 K that mainly exhibit well-developed (111) surface facets, the adsorption behavior is again different [10]. These measurements could be repeated several times indicating that significant structural changes of the particles were absent - which seems reasonable at the low temperatures applied. Our adsorption study clearly demonstrates the need to characterize adsorbates under reaction conditions. If this is carried out under several bars of pressure and at higher temperature even more pronounced effects are expected.

PHOTOCHEMISTRY ON METAL AGGREGATES

In addition to thermal studies of reactivity, nano-sized transition metal aggregates lend themselves to photochemical studies, in which the influence of size and morphology on the photochemistry on the surface of the particles is explored [6, 9, 127]. By changing the formation conditions the geometrical and electronic structure of the metal aggregates can be controlled. The cleavage of an intra-molecular bond by laser irradiation is of particular interest for the rather inert molecule methane. Methane will become an increasingly important raw material, when natural petrol sources will run out [128]. The primary step of methane conversion to methanol or other hydrocarbons [129] is the cleavage of the C-H bond requiring a dissociation energy of 4.5 eV [130]. Even a higher energy of 8.5 eV is necessary for a photochemical cleavage as the first optical allowed transition leading to bond breaking is situated in the vacuum UV.

On the other hand, it has been recently discovered that methane physisorbed on Pt(111) and Pd(111) single crystal surfaces is readily dissociated into methyl and hydrogen by 193-nm (6.42 eV) ArF excimer laser irradiation, [129, 131, 132]. This strong shift of more than 2.1 eV is surprising in view of the low methane surface interaction of around 230-250 meV. Controlled experiments showed that the electronic states of the metal surfaces play an important role in the photo excitation of methane [131, 133].

By using the same systems as discussed before, the influence of Pd cluster size and morphology on the photochemistry of methane was investigated [134]. The average diameter ranged from 1 to 7 nm as determined by spot profile analysis SPA-LEED analysis. We found that the photo reactions strongly depend on the cluster size. In these experiments deuterated methane was photo dissociated by irradiation from excimer laser run at a repetition rate of 4 Hz, a fluence of 2.5 mJ/cm^2 at a photon energy of 6.4 eV, for further experimental details we refer to [135].

As the surface area grows with increasing Pd-deposition a temperature programmed desorption (TPD) spectrum of a saturation coverage of deuterated methane was recorded as a measure of the total surface area available for methane adsorption prior to each photochemistry experiment. For a bare alumina surface no methane desorption peak was observed. The maximum temperature for the TPD spectra did not exceed 300 K. The maximum of the main desorption peak of undissociated methane shifts continuously towards lower temperature with decreasing cluster size. The

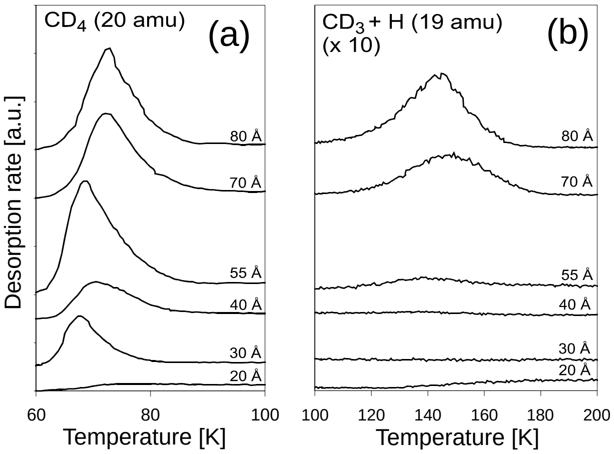

Figure 24. a) Series of (m = 20 amu) TPD spectra after exposure to $1.8\cdot10^{19}$ photons/cm^2 of 6.4°eV depending on Pd-cluster size. b) number of (m = 19 amu) TPD spectra (recombinative desorption of deuterated methyl plus hydrogen) at otherwise same conditions as in a).

TPD spectra of the smallest aggregates (1 nm) were shifted by 10 K as compared to the largest ones (7 nm) indicating a decrease of molecule surface interaction with decreasing cluster size. The peak area of the feature of CD_4 (m = 20 amu) was further used as reference for the total changes in methane concentration due to photon induced dissociation and desorption.

Starting with saturation coverage of deuterated methane the system was exposed to a fixed number of photons impinging on the surface. Figure 24a shows a number of TPD spectra after exposure to $1.8\cdot10^{19}$ photons/cm^2 as a function of Pd aggregate size and is due to undissociated deuterated methane. The maximum of the TPD spectra for (m = 20 amu) turned out to be very sensitive to the coverage, the average cluster size and also coadsorbates like atomic hydrogen from photo dissociation which explains the different shifts of the main feature in those TPD spectra.

In Fig. 24b the recombinative desorption of CD_3H (m = 19 amu) is displayed. The hydrogen on the surface results from residual gas within the chamber and is due to the high sorptivity of palladium with respect to hydrogen adsorption. As it turned out the background free TPD spectra of CD_3H were valuable for the photo dissociation analysis particularly, in case only small photo dissociation rates were observed. No other reaction products have been observed except for the mentioned recombinative desorption of CD_3+H/D.

The residual amount of methane (Fig. 24a) after laser light exposure if related to the initial coverage is a direct measure for the photon induced depletion rate. This loss is mainly contributed by photo desorption and is plotted in dependence of the cluster size in Fig. 25a. Obviously, for small clusters photo desorption (the negligible contribution of photo dissociated methane will be discussed below) is very pronounced, characterized by a cross section of $1\cdot10^{-19}$ cm^2. For increasing cluster size the photon induced desorption becomes more and more ineffective and the cross section reaches a value below $1\cdot10^{-20}$ cm^2, which is also typical from single crystal measurements [136].

The recombinative desorption of CD_3H at around 150 K (Fig 24b) related again to the initial CD_4 coverage before laser light exposure describes the photon reaction rate and is plotted versus the Pd aggregate size in the Fig. 25b. Evidently only above a threshold size of 40 Å photon dissociation starts (cross section of 10^{-22} cm^2) and reaches a value of nearly 10% of the adsorbed methane for the biggest cluster size investigated. This value cannot be exceeded by further photon exposure and is still far below the observed turnover of 80% for Pd(111) [131, 137]. The incomplete turnover of the adsorbed methane by photo dissociation is attributed in case of single crystals to the evolving product concentration on the metal surface [138]. According to IR-measurements the increasing CH_3-coverage reduces the interaction of methane with the surface. As seen above, this self quenching is also observed for photochemistry on the Pd-clusters. However, it occurs at much lower concentrations. For the largest aggregates in our experiments for which the overall photo reaction cross section approaches the value of $7\cdot10^{-21}$ cm^2 as for the single crystal surface, but ca. 85% of the initial coverage remained unreacted.

Single crystal experiments have shown that the initial excitation step is likely to occur within the adsorbate. Two models are actually discussed in the literature to explain the laser induced dissociation of methane on Pt(111) and Pd(111) [131, 137, 139].

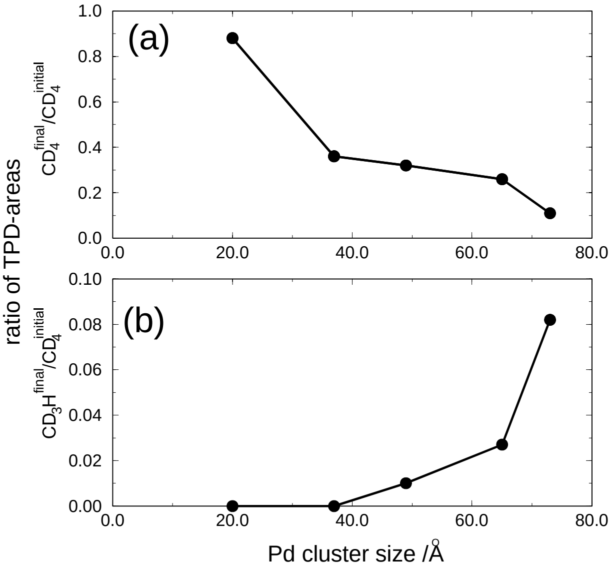

Figure 25. a) Plot of overall reaction loss of undissociated CD_4 normalized to the initial coverage as a function of Pd-cluster size. b) Plot of CD_3H formation ratio in respect to the initial coverage depending on the Pd-cluster size.

The first model [131] is supported by ab initio cluster calculations for Pt (clusters from 1-10 atoms) [139]. It discusses a mixing of the unoccupied anti-bonding Rydberg state of methane (gas phase value: 8.5 eV) with unoccupied metal states to account for a broadening and a shift of the first electronically excited state so that the photo dissociation at 6.4 eV becomes possible. The excitation energy of this state leading to dissociation to CH_3 + H is strongly depending on the cluster size as the electron redistribution over the surrounding metal plays an important role to stabilize this charge transfer state [139]. Within this model a decrease of the cluster size causes a reduction of the delocalisation resulting in a shift of the excitation energy towards higher energies.

The second model argues that a reduction of the ionization potential of methane due to the interaction with the metal accounts for the possibility to dissociate methane at 6.4 eV [137]. Starting from the vacuum level of Pd the Fermi level of the metal is situated 5.6 eV below the vacuum level according to work function measurements [140]. With reference to the vacuum level the HOMO (highest occupied molecular orbital) state of methane is 12.6 eV below the vacuum level considering the gas phase value [140]. A further attractive force due to the image charge resulting from the ionic excited state further stabilizes this level by a shift towards the vacuum level [137]. Slab LDA calculations on CH_4/Pd(111) revealed that the equilibrium height between the Pd plane to the C nucleus of 3 Å above the surface [137] allows to use the image charge model of Jennison et al. [141] from which an estimate of 1.9 eV can be made for the attractive force. Assuming a low electron tunneling barrier between adsorbate and substrate one obtains an approximate minimum excitation energy of 5.1 eV to produce the dissociative state of cationic methane. Indeed no photo dissociation could be observed on single crystals at excitation energies of 5.0 eV [129, 132]. The image potential will be strongly depending on the electronic structure and thus on the cluster size which explains a decrease in photo dissociation probability. Furthermore, as the image-potential changes scale with $1/r$ (r being the equilibrium height of CH_4 above Pd), the dissociation efficiency might be strongly influenced by the cluster size which governs the actual interaction between methane and the substrate. This is supported by the observation that the peak maxima of TPD spectra of the undissociated methane shift towards lower temperatures with decreasing cluster size indicative for a diminishing interaction between the molecules and the surface thus increasing molecule-surface distance.

Intuitively, one expects an increased lifetime of the excited state concomitant with the quantisation of the electronic states when reducing the cluster size which would increase the photo dissociation probability. However, this effect appears to be less important than the influence of charge delocalisation within the cluster on the photo dissociation threshold.

In summary, photo dissociation, and photo desorption of methane at λ = 193 nm on the Pd-clusters of various sizes on a thin epitaxial Al_2O_3 support show very pronounced size effects and remarkable differences from the Pd(111) single crystal results. These results strongly suggest that metal clusters of different sizes and shapes provide a unique way for controlling both photochemical and thermal reactions of hydrocarbons at metal surfaces.

SYNOPSIS

We have demonstrated in the present review how surface science tools and ideas can be used to prepare and study model systems for heterogeneous catalysts. In our view it seems possible to bridge the so called materials as well as the pressure gaps between surface science and catalysis. This opens fruitful avenues for surface science. Surface science which was, when Wyn Roberts entered this field, in its infancy beginning has developed into a mature science thanks to scientists of his stature, and there is still room for the development of strategies as well as methods to let our field prosper and keep it very much alive in the future.

ACKNOWLEDGEMENTS

We are grateful to our coworkers, whose names appear in the references for their contributions to the work summarized in this paper. A number of funding agencies have helped to perform the research described here. Among them are Max-Planck-Gesellschaft, Deutsche Forschungsgemeinschaft, Bundesministerium für Bildung und Forschung, COST, European Union, German Israeli Foundation, as well as the NEDO International Joint Research Grant on Photon and Electron Controlled Surface Processes. We thank them for their support.

REFERENCES

[1] 12th International Congress on Catalysis, Studies in Surface Science and Catalysis, edited by A. Corma, F.V. Melo, S. Mendioroz and J.L.G. Fierro (Elsevier, Amsterdam, 2000).
[2] H.-J. Freund, Faraday Disc., 114 (1999) 1.
[3] M. Bäumer and H.-J. Freund, Progr. Surf. Sci., 61 (1999) 127.
[4] H.-J. Freund, M. Bäumer and H. Kuhlenbeck, Adv. Catal., 45 (2000) 412.
[5] D.W. Goodman, Surf. Rev. Lett., 2 (1995) 9.
[6] C.R. Henry, Surf. Sci. Rep., 31 (1998) 231.
[7] U. Diebold, J.-M. Pan and T.E. Madey, Surf. Sci., 331-333 (1995) 845.
[8] P.J. Møller and J. Nerlov, Surf. Sci., 307-309 (1993) 591.

[9] H.-J. Freund, Angew. Chem. Int. Ed. Engl., 36 (1997) 452.
[10] T. Dellwig, G. Rupprechter, H. Unterhalt and H.-J. Freund, Phys. Rev. Lett., 85 (2000) 776.
[11] C.T. Au and M.W. Roberts, Nature, 319 (1986) 206.
[12] M.W. Roberts, Appl. Surf. Sci., 52 (1991) 133.
[13] R.B. Moyes and M.W. Roberts, J. Catal., 49 (1977) 216.
[14] M.W. Roberts, Chem. Soc. Rev., 18 (1989) 451.
[15] M.W. Roberts, Chem. Soc. Rev., 25 (1996) 437.
[16] R.W. Joyner and M.W. Roberts, Chem. Phys. Lett., 29 (1974) 447.
[17] M.W. Roberts and R.S.C. Smart, Surf. Sci., 100 (1980) 590.
[18] S.J. Atkinson, C.R. Brundle and M.W. Roberts, Faraday Disc., 58 (1974) 62.
[19] M.W. Roberts and R.S.C. Smart, J. Chem. Soc., Faraday Trans. 1, 80 (1984) 2957.
[20] M.W. Roberts and R.S.C. Smart, Surf. Sci., 151 (1985) 1.
[21] M.W. Roberts and R.S.C. Smart, Chem. Phys. Lett., 69 (1980) 234.
[22] H. Schmalzried, Chemical Kinetics of Solids, (Verlag Chemie, Weinheim, 1995).
[23] R.K. Grasselli and J.D. Burrington, Adv. Catal., 30 (1981) 133.
[24] F. Cavani, G. Centi, F. Trifiro and R.K. Grasselli, Catal. Today, 3 (1988) 185.
[25] P.A. Agaskar, L. DeCaul and R.K. Grasselli, Catal. Lett., 23 (1994) 339.
[26] B. Tepper, PhD-Thesis, Freie Universität, Belrin, in preparation.
[27] A.-C. Dupuis, PhD-Thesis, Humboldt Universität, Berlin, in preparation.
[28] K. Hermann, M. Witko, R. Druzinic, A. Chakrabarti, B. Tepper, M. Elsner, A. Gorschlüter, H. Kuhlenbeck and H.-J. Freund, J. Electron Spectrosc. Relat. Phenom., 98-99 (1999) 245.
[29] M. Figlarz, Progr. Solid State Chem., 19 (1989) 1.
[30] G. Renaud, Surf. Sci. Rep., 32 (1998) 1.
[31] F. Rohr, M. Bäumer, H.-J. Freund, J.A. Mejias, V. Staemmler, S. Müller, L. Hammer and K. Heinz, Surf. Sci., 372 (1997) L 291.
[32] F. Rohr, M. Bäumer, H.-J. Freund, J.A. Mejias, V. Staemmler, S. Müller, L. Hammer and K. Heinz, Surf. Sci., 389 (1997) 391.
[33] S.K. Shaikhoutdinov and W. Weiss, Surf. Sci., 432 (1999) L627.
[34] X.-G. Wang, W. Weiss, S.K. Shaikhoutdinov, M. Ritter, M. Petersen, F. Wagner, R. Schlögl and M. Scheffler, Phys. Rev. Lett., 81 (1998) 1038.
[35] N.M. Harrison, X.-G. Wang, J. Muscat and M. Scheffler, Faraday Disc., 114 (1999) 305.
[36] K. Wolter, D. Scarano, J. Fritsch, H. Kuhlenbeck, A. Zecchina and H.-J. Freund, Chem. Phys. Lett., 320 (2000) 206.

[37] B. Dillmann, F. Rohr, O. Seiferth, G. Klivenyi, M. Bender, K. Homann, I.N. Yakovkin, D. Ehrlich, M. Bäumer, H. Kuhlenbeck and H.-J. Freund, Faraday Disc. 105, (1996) 295.
[38] C. Xu, B. Dillmann, H. Kuhlenbeck and H.-J. Freund, Phys. Rev. Lett., 67 (1991) 3551.
[39] M. Pykavy, V. Staemmler, O. Seiferth and H.-J. Freund, Surf. Sci., (submitted).
[40] A.F. Carley, D.E. Gallagher and M.W. Roberts, Spectrochim. Acta, 43 (1987) 1447.
[41] R.G. Copperthwaite, P.R. Davies, M.A. Morris, M.W. Roberts and R.A. Ryder, Catal. Lett., 1 (1988) 11.
[42] H.-J. Freund and M.W. Roberts, Surface Science Reports, 25 (1996) 225.
[43] O. Seiferth, K. Wolter, B. Dillmann, G. Klivenyi, H.-J. Freund, D. Scarano and A. Zecchina, Surf. Sci., 421 (1999) 176.
[44] M.-C. Wu and P.J. Møller, Surf. Sci., 224 (1989) 250.
[45] H. Poppa, Catal. Rev. Sci. Eng., 35 (1993) 359.
[46] M. Heemeier, M. Frank, J. Libuda, K. Wolter, H. Kuhlenbeck, M. Bäumer and H.-J. Freund, Catal. Lett., 68 (2000) 19.
[47] J. Libuda, F. Winkelmann, M. Bäumer, H.-J. Freund, T. Bertrams, H. Neddermeyer and K. Müller, Surf. Sci., 318 (1994) 61.
[48] N. Ernst, B. Duncombe, G. Bozdech, M. Naschitzki and H.-J. Freund, Ultramicroscopy, 79 (1999) 231.
[49] K.H. Hansen, T. Worren, S. Stempel, E. Lægsgaard, M. Bäumer, H.-J. Freund, F. Besenbacher and I. Stensgaard, Phys. Rev. Lett., 83 (1999) 4120.
[50] N. Nilius, A. Cörper, G. Bozdech, N. Ernst and H.-J. Freund, Progr. Surf. Sci., (in press).
[51] G.L. Kellogg, Surf. Sci. Rep., 21 (1994) 1.
[52] A. Cörper, G. Bozdech, N. Ernst and H.-J. Freund (unpublished).
[53] A. Bogicevic and D.R. Jennison, Phys. Rev. Lett., 82 (1999) 4050.
[54] A. Piednoir, E. Perrot, S. Granjeaud, A. Humbert, C. Chapon and C.R. Henry, Surf. Sci., 391 (1997) 19.
[55] M. Methfessel, D. Hennig and M. Scheffler, Phys. Rev. B, 46 (1992) 4816.
[56] A. Sandell, J. Libuda, P.A. Brühwiler, S. Andersson, M. Bäumer, A.J. Maxwell, N. Mårtensson and H.-J. Freund, Phys. Rev. B, 55 (1997) 7233.
[57] A. Bettac, L. Köller, V. Rank and K.H. Meiwes-Broer, Surf. Sci., 402 (1998) 475.
[58] M. Valden, X. Lai and D.W. Goodman, Science, 281 (1998) 1647.
[59] B.C. Stipe, M.A. Rezaei and W. Ho, Science, 280 (1998) 1732.
[60] J.H. Coombs, J.K. Gimzewski, B. Reihl, J.K. Sass and R.R. Schlittler, J. Microscopy, 152 (1988).

[61] R. Berndt, in Scanning Probe Microscopy, edited by R. Wiesendanger, Springer Series Nanoscience and Technology (Springer, Berlin, 1998), page 97.
[62] N. Nilius, N. Ernst and H.-J. Freund, Phys. Rev. Lett., 84 (2000) 3994.
[63] Optical Properties of Metal Clusters, edited by U. Kreibig and M. Vollmer, Springer Series in Materials Science, Vol. 25 (Springer, Berlin, 1995).
[64] N. Nilius, N. Ernst, H.-J. Freund and P. Johansson, Phys. Rev. B, 61 (2000) 12682.
[65] A. Liebsch, Phys. Rev. B, 48 (1993) 11317.
[66] H. Schlienz, M. Beckendorf, U.J. Katter, T. Risse and H.-J. Freund, Phys. Rev. Lett., 74 (1995) 761.
[67] U.J. Katter, T. Hill, T. Risse, H. Schlienz, M. Beckendorf, T. Klüner, H. Hamann and H.-J. Freund, J. Phys. Chem. B, 101 (1997) 552.
[68] T. Risse, T. Hill, J. Schmidt, G. Abend, H. Hamann and H.-J. Freund, J. Chem. Phys., 108 (1998) 8615.
[69] T. Hill, M. Mozaffari-Afshar, J. Schmidt, T. Risse, S. Stempel, M. Heemeier and H.-J. Freund, Chem. Phys. Lett., 292 (1998) 524.
[70] T. Hill, S. Stempel, T. Risse, M. Baeumer and H.-J. Freund, J. Magn. Mag. Mater., 198-199 (1999) 354.
[71] T. Hill, PhD-Thesis, Ruhr-Universität Bochum, 1998.
[72] D.R. Rainer and D.W. Goodman, in Chemisorption and Reactivity on Supported Clusters and Thin Films, edited by R. M. Lambert and G. Pacchioni, Series E, Vol. 331 (Kluwer, Dordrecht, 1997), page 27.
[73] I. Meusel, J. Hoffmann, J. Hartmann, M. Heemeier, M. Bäumer, J. Libuda and H.-J. Freund, Catal. Lett., (submitted).
[74] J. Libuda, I. Meusel, J. Hartmann and H.-J. Freund, Rev. Sci. Instrum., (accepted).
[75] E. Gillet, S. Channakhone, V. Matolin and M. Gillet, Surf. Sci., 152/153 (1985) 603.
[76] I. Stará, V. Nehasil and V. Matolin, Surf. Sci., 365 (1996) 69.
[77] C. Becker and C.R. Henry, Surf. Sci., 352 (1996) 457.
[78] C. Becker and C.R. Henry, Catal. Lett., 43 (1997) 55.
[79] V.P. Zhdanov and B. Kasemo, J. Catal., 170 (1997) 377.
[80] V.P. Zhdanov and B. Kasemo, Surf. Sci., 405 (1998) 27.
[81] V.P. Zhdanov and B. Kasemo, Phys. Rev. B, 55 (1997) 4105.
[82] C.R. Henry, Surf. Sci., 223 (1991) 519.
[83] D.A. King and M.G. Wells, Proc. Roy. Soc. Ser. A, 339 (1974) 245.
[84] D.A. King and M.G. Wells, Surf. Sci., 29 (1972) 454.
[85] M. Bäumer, J. Libuda and H.-J. Freund, in Chemisorption and Reactivity on Supported Clusters and Thin Films, edited by R. M. Lambert and G. Pacchioni, NATO ASI Series E, Vol. 331 (Kluwer, Dordrecht, 1997), page 61.
[86] J. Libuda, PhD-Thesis, Ruhr-Universität Bochum, 1996.
[87] T. Engel, J. Chem. Phys., 69 (1978) 373.

[88] C.T. Rettner, D.J. Auerbach, J.C. Tully and A.W. Kleyn, J. Phys. Chem., 100 (1996) 13021.
[89] J.A. Barker and D.J. Auerbach, Surf. Sci. Rep., 4 (1985) 1.
[90] T. Dellwig, J. Hartmann, J. Libuda, I. Meusel, G. Rupprechter, H. Unterhalt and H.-J. Freund, J. Mol. Catal., (accepted).
[91] I. Stará, V. Nehasil and V. Matolin, Surf. Sci., 331 (1995) 173.
[92] D.L. Weissman, M.I. Shek and W.E. Spicer, Surf. Sci., 92 (1980) L59.
[93] P. Legare, L. Hilaire, G. Maire, G. Krill and A. Amamou, Surf. Sci., 107 (1981) 533.
[94] D.L. Weissman-Wenicur, M.L. Shek, P.M. Stefan, I. Lindau and W.E. Spicer, Surf. Sci., 127 (1983) 513.
[95] L. Surnev, G. Bliznakov and M. Kiskinova, Surf. Sci., 140 (1984) 249.
[96] R. Imbihl and J.E. Demuth, Surf. Sci., 173 (1986) 395.
[97] B. Oral and R.W. Vook, Appl. Surf. Sci., 29 (1987) 20.
[98] M. Milun, P. Pervan, M. Vacjic and K. Wandelt, Surf. Sci., 211-212 (1989) 887.
[99] X. Guo, A. Hoffman and J.T. Yates, Jr., J. Chem. Phys., 90 (1989) 5787.
[100] B.A. Banse and B.E. Koel, Surf. Sci., 232 (1990) 275.
[101] V.A. Bondzie, P. Kleban and D.J. Dwyer, Surf. Sci., 347 (1996) 319.
[102] P. Sjövall and P. Uvdal, Chem. Phys. Lett., 282 (1998) 355.
[103] P. Sjövall and P. Uvdal, J. Vac. Sci. Technol. A, 16 (1998) 943.
[104] E.H. Voogt, A.J.M. Mens, O.L.J. Gijzeman and J.W. Geus, Surf. Sci., 373 (1997) 210.
[105] W. Huang, R. Zhai and W. Bao, Surf. Sci., 439 (1999) L803.
[106] F.P. Leisenberger, G. Koller, M. Sock, S. Surnev, M.G. Ramsey, F.P. Netzer, B. Klötzer and K. Hayek, Surf. Sci., 445 (2000) 380.
[107] M. Eriksson and L.G.M. Pettersson, Surf. Sci., 311 (1994) 139.
[108] H. Graoui, S. Giorgio and C.R. Henry, Surf. Sci., 417 (1998).
[109] M. Eriksson, L. Olsson, U. Helmersson, R. Erlandsson and L.-G. Ekedahl, Thin Solid Films, 342 (1999) 297.
[110] S. Ladas, R. Imbihl and G. Ertl, Surf. Sci., 219 (1989) 88.
[111] M.R. Bassett and R. Imbihl, J. Chem. Phys., 93 (1990) 811.
[112] T. Engel and G. Ertl, J. Chem. Phys., 69 (1978) 1267.
[113] T. Engel and G. Ertl, in The Chemical Physics of Solid Surfaces and Heterogeneous Catalysis, edited by D. A. King and D. P. Woodruff, Vol. 4 (Elsevier, 1982), page 73.
[114] I.Z. Jones, R.A. Bennett and M. Bowker, Surf. Sci., 439 (1999) 235.
[115] V.P. Zhdanov and B. Kasemo, Surf. Sci. Rep., 39 (2000) 25.
[116] J. Libuda, I. Meusel, J. Hoffmann, J. Hartmann, M. Piccolo, C.R. Henry and H.-J. Freund, J. Chem. Phys., (submitted).
[117] J.A. Jensen, K.B. Rider, M. Salmeron and G.A. Somorjai, Phys. Rev. Lett., 80 (1998) 1228.

[118] G.A. Somorjai and G. Rupprechter, J. Phys. Chem. B, 103 (1999) 1623.

[119] G. Rupprechter, T. Dellwig, H. Unterhalt and H.-J. Freund, Topics in Catalysis, (in press (2001)).

[120] Y.R. Shen, Surf. Sci., 299/300 (1994) 551.

[121] J. Miragliotta, P. Rabinowitz, S.D. Cameron and R.B. Hall, Appl. Phys. A, 51 (1990) 221.

[122] M. Bäumer, J. Libuda, A. Sandell, H.-J. Freund, G. Graw, T. Bertrams and H. Neddermeyer, Ber. Bunsenges. Phys. Chem., 99 (1995) 1381.

[123] F.M. Hoffmann, Surf. Sci. Rep., 3 (1983) 103.

[124] M. Tüshaus, W. Berndt, H. Conrad, A.M. Bradshaw and B. Persson, Appl. Phys. A, 51 (1990) 91.

[125] W.K. Kuhn, J. Szanyi and D.W. Goodman, Surf. Sci. Lett., 274 (1992) L611.

[126] A.M. Bradshaw and F.M. Hoffmann, Surf. Sci., 52 (1975) 449.

[127] C.T. Campbell, Surf. Sci. Rep., 27 (1997) 1.

[128] K. Seshan and J.A. Lercher, in Carbon Dioxide Chemistry: Environmental Issues, edited by J. Paul and C.-M. Pradier (The Royal Society of Chemistry, 1994).

[129] Y.A. Gruzdkov, K. Watanabe, K. Sawabe and Y. Matsumoto, Chem. Phys. Lett., 227 (1994) 243.

[130] K.-P. Huber and G. Herzberg, Molecular Spectra and Molecular Structure, IV. Constants of Diatomic Molecules, (Van Nostrand Reinhold, New York, 1979).

[131] Y. Matsumoto, Y.A. Gruzdkov, K. Watanabe and K. Sawabe, J. Chem. Phys., 105 (1996) 4775.

[132] K. Watanabe and Y. Matsumoto, Surf. Sci., 390 (1997) 250.

[133] K. Watanabe, K. Sawabe and Y. Matsumoto, Phys. Rev. Lett., 76 (1996) 1751.

[134] K. Watanabe, Y. Matsumoto, M. Kampling, K. Al-Shamery and H.-J. Freund, Angew. Chem. Int. Ed., 38 (1999) 2192.

[135] M. Kampling, PhD-Thesis, Freie Universität, 2000.

[136] K. Watanabe, PhD-Thesis, Institute of Molecular Physics, Okasaki, 1997.

[137] D.R. Jennison, private communication.

[138] J. Yoshinobu, H. Ogasawa and M. Kawai, Phys. Rev. Lett., 75 (1995) 2176.

[139] Y. Akinaga, T. Taketsugu and T. Hirao, J. Chem. Phys., 107 (1997) 415.

[140] Handbook of Chemistry and Physics, edited by D.R. Lide (CRC Press, Boca Raton, 1997-1998).

[141] D.R. Jennison, E.B. Stechel, A.R. Burns and Y.S. Li, Nucl. Instr. Meth. Phys. Res., B101 (1995) 22.